

THESIS

SYNTHESIS AND CHARACTERIZATION OF LITHIUM-ION CATHODE MATERIALS IN

THE SYSTEM  $(1-x-y) \text{LiNi}_{0.8}\text{Co}_{0.15}\text{Al}_{0.05}\text{O}_2 \cdot x\text{Li}_2\text{MnO}_3 \cdot y\text{LiCoO}_2$

Submitted by

Anish Yerramilli

Department of Mechanical Engineering

In partial fulfillment of the requirements

For the Degree of Master of Science

Colorado State University

Fort Collins, Colorado

Fall 2013

Master's Committee:

Advisor: Susan P. James

Amy Prieto  
Mingzhong Wu

## ABSTRACT

### SYNTHESIS AND CHARACTERIZATION OF LITHIUM-ION CATHODE MATERIALS IN THE SYSTEM $(1-x-y)$ $\text{LiNi}_{0.8}\text{Co}_{0.15}\text{Al}_{0.05}\text{O}_2 \cdot x\text{Li}_2\text{MnO}_3 \cdot y\text{LiCoO}_2$

Energy storage technology has been dominated by lithium ion batteries, which are considered the most promising with higher energy density compared to any other battery technologies. The market for lithium ion batteries has increased rapidly from 2007. Goals set by the U.S Department of Energy for hybrid electric vehicles have not been met by any of the existing cathode materials.

The objective of this thesis was to find a material composition that has better cyclability and lower cost than the standard battery materials. A ternary composition with low cost materials like Al, Mn and Ni were used instead of high amounts of Co to reduce the cost of the battery. It was hypothesized that there are cathode compositions in the system  $(1-x-y)$   $\text{LiNi}_{0.8}\text{Co}_{0.15}\text{Al}_{0.05}\text{O}_2 \cdot x\text{Li}_2\text{MnO}_3 \cdot y\text{LiCoO}_2$  that when tested for discharge capacities and cyclability will show better properties than the current generation lithium ion cathode materials.

The system  $(1-x-y)$   $\text{LiNi}_{0.8}\text{Co}_{0.15}\text{Al}_{0.05}\text{O}_2 \cdot x\text{Li}_2\text{MnO}_3 \cdot y\text{LiCoO}_2$  is synthesized using a simple sol-gel synthesis. The materials  $\text{LiNi}_{0.8}\text{Co}_{0.15}\text{Al}_{0.05}\text{O}_2$ ,  $\text{Li}_2\text{MnO}_3$  and  $\text{LiCoO}_2$  were used as end points in a ternary composition diagram. Twenty eight cathode compositions spanning the entire ternary composition diagram were synthesized under the same conditions and characterized using X-ray diffraction (XRD) and an Arbin BT2000 battery testing system.

XRD results showed  $\alpha\text{-NaFeO}_2$  structure with a space group of R3m. The results from electrochemical testing revealed a wide range of electrochemical capacities and cyclabilities. The regions close to  $\text{Li}_2\text{MnO}_3$  showed high capacities and cyclability. The material with composition

$\text{Li}_{1.5}\text{Ni}_{0.133}\text{Co}_{0.358}\text{Al}_{0.008}\text{Mn}_{0.5}$  had an initial discharge capacity of 216.3 mAh/g and retained this capacity even after multiple cycles in the voltage range of 4.6-2 V at a rate of C/15.

Statistical analysis was done using SAS/STAT 9.2 with the ADX procedure to fit a general linear model with three linear terms and three two way interactions to map capacities and cyclabilities. This analysis was used to choose the compositions with best capacities and cyclability. Inductively couple plasma (ICP) analysis was carried out on the chosen samples to find the error between calculated composition and the theoretical composition. XPS (X-ray photoelectron spectroscopy) was conducted for the chosen samples and the oxidation states of the elements were determined.

The material with composition  $\text{Li}_{1.5}\text{Ni}_{0.133}\text{Co}_{0.358}\text{Al}_{0.008}\text{Mn}_{0.5}$  was found to be the promising material for commercialization. Before going into the market additional changes like synthesis conditions and surface treatments should be conducted on the material.

## ACKNOWLEDGEMENTS

I want to thank my advisor, Dr. Susan P. James for being the one to support my research work and giving me invaluable guidance over the last year. I would also like to thank Dr. Amy Prieto and Dr. Mingzhong Wu for agreeing to serve on my committee. Additionally, I would like to thank Dr. Sandeep Kohli and Dr. Pat McCurdy from the department of chemistry for helping me with different characterization techniques. My colleagues Brandon Kelly, Rushendra Paravasthu , Madhu Channabasappa, Josh Garrett, Bhavin Patel, Mike Yeager and Siddharth Paravasthu all have played an important role in my research work and were always helpful. Finally, thanks to my family and friends for always being there for me and for supporting me in whatever I do.

## TABLE OF CONTENTS

### Chapter 1 Introduction

1.1 Motivation of Research.....	1
1.1.1 Manufacturer.....	1
1.1.2 Patents on Battery Technology.....	2
1.1.3 Competing Technologies.....	2
1.1.4 Scope of work.....	5
1.2 Basics of Li ion technology.....	6
1.3 History of Technology.....	7
1.4 Lithium ion battery anodes.....	9
1.5 Electrolytes.....	11
1.6 Battery Design and Commercialization.....	13

### Chapter 2 Cathode Materials

2.1 History of cathode materials.....	17
2.2 Olivine and Spinel structure cathodes.....	18
2.3 Layered Compounds.....	20

### Chapter 3 Experimental Methods

3.1 Solid State Synthesis.....	27
3.2 Sol-gel Synthesis.....	28
3.3 Characterization .....	29
3.3.1 X-ray diffraction.....	29
3.3.2 Differential Scanning Calorimeter.....	29

3.3.3 ICP/AES.....	29
3.4 Half Cell Assembly.....	34
3.5 Full Cell Assembly.....	35
3.6 Electrochemical Testing.....	36
<b>Chapter 4 Objectives, Approach and Scope.....</b>	<b>37</b>
4.1 Thesis Statement.....	37
4.2 Objectives.....	37
4.3 Approach.....	39
<b>Chapter 5 Results and Discussion</b>	
5.1 System Overview.....	40
5.2 XRD.....	43
5.3 Electrochemical Testing.....	48
5.4 Statistical Analysis.....	54
5.5 ICP-AES.....	57
5.6 Repeats.....	58
5.7 XPS.....	60
5.8 Discussion of Best compositions.....	61
<b>Chapter 6 Conclusions and Future work.....</b>	<b>67</b>
<b>References.....</b>	<b>70</b>

# Chapter 1 Introduction

## *1.1 Motivation of Research*

### *1.1.1 Manufacturers*

Since the introduction of the automobile, engineers and designers have been searching for ways to make them more efficient and save on fuel consumption. Rising pollution levels caused in part by internal combustion engine vehicles have led to the advent of zero emission vehicles. Batteries with high efficiency, cycleability and safety are needed for energy storage in these zero emission vehicles.

Lithium ion batteries are the most promising energy storage technology with higher energy density compared to other battery technologies. While the cost of the battery continues to decrease, the safety and cycling issues continue to improve. Lithium ion is a low maintenance battery, an advantage that most other chemistries cannot claim. There is no memory and no scheduled cycling is required to prolong the battery's life

The market for lithium ion batteries has increased rapidly from 2007. President Barack Obama announced \$2.4 billion for the Advanced Battery Manufacturing Initiative (ABMI) on March 19, 2009[1]. This recovery act will fund 48 new advanced battery and electric drive components manufacturing and electric drive vehicle deployment projects in over 20 states. It is estimated that the global market for lithium ion batteries could grow from \$877 million in 2010 to \$8 billion by 2015. In North America, the market is expected to expand from about \$287 million in 2010 to \$2.2 billion in 2015. [1]

The companies that got funding from ABMI include A123Systems, which would build a \$600-million, 844-employee plant in the Detroit-metro suburb of Livonia; Compact Power, an alliance

between LG Chem and General Motors, which would construct a \$200-million, 300-employee plant at an undetermined site in Michigan State; Johnson Controls-Saft Advanced Power Solutions, which would invest \$220 million and add 498 new employees making Li-ion batteries at an existing plant in Holland, Michigan and KD Advanced Battery Group, a partnership of Dow Chemical, Kokam America and Townsend Ventures, which would build a new \$665-million, 845-employee plant at an as-yet undetermined Michigan location.[2]. These companies are enhancing their research departments to improve the efficiency of the batteries while decreasing the costs for manufacturing. But, most of the companies are still unsuccessful in achieving significant progress in the field leaving behind a great opportunity for research.

### *1.1.2 Patents on Battery Technology*

The importance of battery technology can be proved by the advancements in its patents. With growing research in the area of batteries there is a great concern over intellectual property. According to USPTO there are more than 10,000 approved patents in this area until 2010 and out of which 70% of them focus on cathode materials.

### *1.1.3 Competing Technologies*

There are competing technologies for lithium ion batteries: ultra capacitors, hydrogen and other battery technologies. The reasons for not using those technologies in hybrid vehicles are briefly explained in the following paragraphs.

**Table 1. Comparison of Lithium ion battery technologies with other battery technologies[1]**

	Lithium ion	Nickel Metal Hydride	Nickel Cadmium	Lead acid
Working Voltage (v)	3.7	1.2	1.2	2
Gravimetric Energy Density (Wh/Kg)	130~200	60~90	40~60	30~40
Volumetric Energy Density (Wh/L)	340~400	200~250	160~200	130~180
Cycle life	500	400	400	300
Self-discharge rate (% per month)	5	35	30	10
Energy Efficiency ( $C_{\text{discharge}}/C_{\text{charge}}$ )	99%	70%	70%	75%
Weight of the material for the same capacity	1	2	2.5	4
Memory Effect	None	40%	None	None
Reliability	High	Low	Average	High

An ultracapacitor, also known as a double-layer capacitor, polarizes an electrolytic solution to store energy electrostatically. Though it is an electrochemical device, no chemical reactions are involved in its energy storage mechanism. There are disadvantages when considering ultracapacitors for hybrid vehicles. The first and main disadvantage is the fact that they cannot hold power like lithium ion batteries. They also cannot carry the same voltages as regular batteries. With this low working voltage, they are only used in limited applications. [15]

In the case of hydrogen fuel cell vehicles, the primary disadvantage is their storage. Although molecular hydrogen has very high energy density on a mass basis, it has very low energy density by volume because of its low molecular weight. If it is to be used as fuel stored onboard the vehicle, pure hydrogen gas must be pressurized or liquefied to provide sufficient driving range. High cost and questionable safety are also barriers for its use in hybrid vehicles.[16]

Nickel cadmium batteries which are considered to be cheap and have a prolonged life cycle have their disadvantages too. Memory effect is the important one; they tend to remember the discharge capacity which leads to lower capacities during long term use. They are toxic in nature, need to be charged after storage and have relatively low energy density.

Nickel metal hydride batteries are also gaining importance. They have limitations like high self-discharge, high maintenance requirements, limited service life and the performance degrades rapidly if stored at elevated temperatures.

### 1.1.4 Scope of work

The Department of Energy has set some goals for hybrid electric vehicles as shown in Figure 1. Out of the 11 areas to be improved, eight areas have shown progress. The eight areas include discharge pulse power, regenerative pulse power, available energy, efficiency, cycle life, system weight, system volume and self-discharge. The goals which seem to be challenging are unmet; operating temperature from -30C to 52C, a lifetime of 15 years and a selling price below \$500 to \$800 per system at 100,000 units produced per year. This thesis addresses two of those three goals: cost and lifetime. [3]

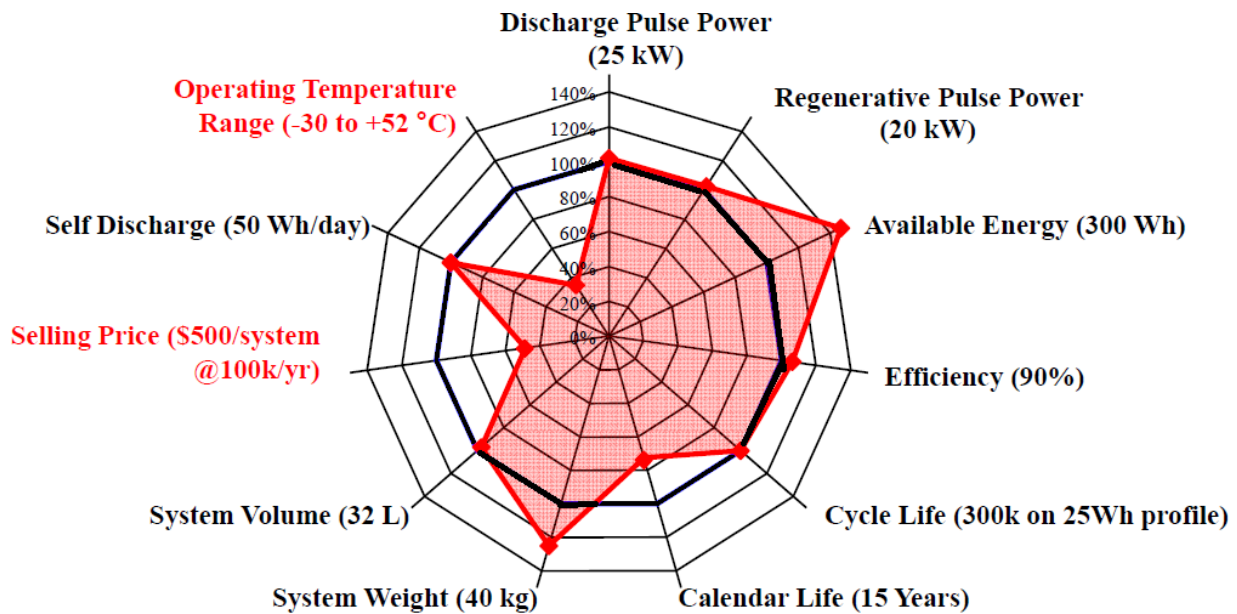


**Figure 1. Goals set for hybrid electric vehicles by Department Of Energy**

Black web indicates the goals to be reached and the red web indicates the current status of goals reached

## 1.2 Basics of Li ion technology

Lithium ion battery consists of a negative electrode (anode), a positive electrode (cathode), electrolyte and a separator which are like the main components for building a battery. The following figure gives a graphical representation and basic terminology of a working battery.

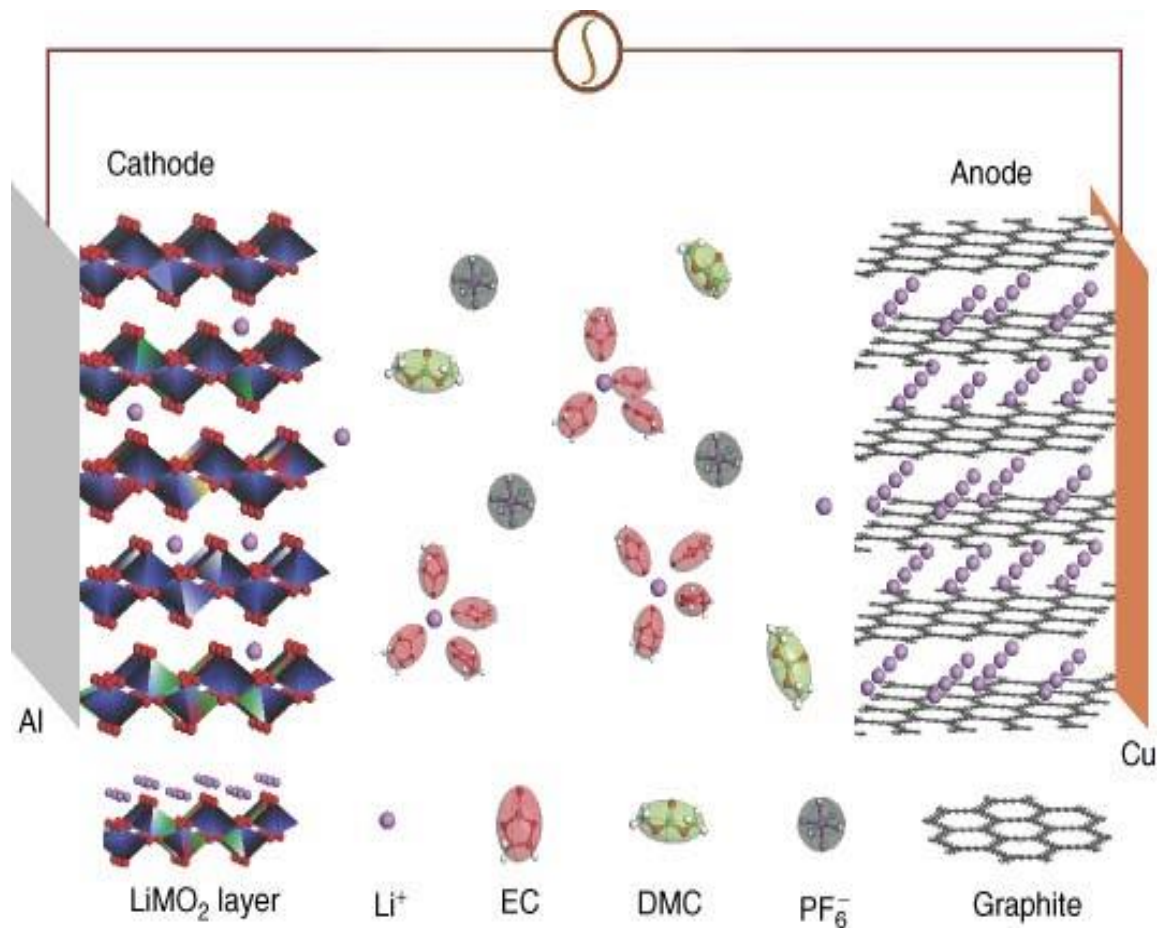
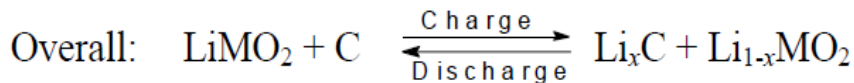
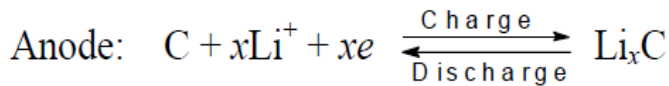
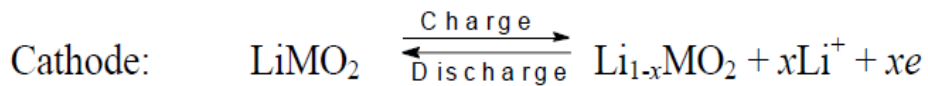


**Figure 2. Working of a basic lithium ion battery[4]**

During charging, lithium ions move from cathode (deintercalation) to electrolyte which is attracted into the anode material (intercalation), electrons are removed from cathode by an external field and transferred to an anode. On discharge, the anode supplies the ions to

electrolyte, electrons to the external circuit where the ions intercalate into electrochemically conducting host cathode and electrons from the external circuit for charge compensation. As this reaction is reversible it is called a “rocking chair” cell. [5]

The following reactions occur during charging and discharging



LiMO<sub>2</sub> represents transitional metal oxide.

### *1.3 History of Technology*

Lithium has a low atomic number and a high electrode potential which results in significantly higher energy density for the lithium ion battery compared to traditional batteries like lead and zinc. The work on lithium ion battery began in 1912 by G.N.Lewis. Lithium-carbon mono fluoride based primary cells were developed by Matsushita in 1973, followed by Sanyo’s commercial lithium-manganese dioxide primary cells in 1975. After 1975, the focus was on developing rechargeable secondary batteries with high energy densities. Using lithium as anode materials caused too many safety concerns; attention was focused on lithium insertion compounds. Lazzari and Scrosati proposed the “rocking chair” concept in 1980 using two

lithium insertion compounds as both positive and negative electrodes. In 1981, Ikeda of Sanyo used graphite as anode material which gave comparable cell voltages as lithium metal cells. Based on the work by Goodenough, Sony Corporation commercialized these batteries using a layered carbon anode and  $\text{LiCoO}_2$  in 1991. In 1996 Goodenough and Akshaya Padhi came up with a new olivine structure cathode material  $\text{LiFePO}_4$ . [6]

High irreversible fading capacity during cycling made  $\text{LiFePO}_4$  an undesirable anode material. Graphite as an anode material had desirable intercalation properties but the early attempts resulted in breaking up of graphite particles because of gas released during the intercalation process. In 1998 as a part of 1<sup>st</sup> generation battery technology, Ube Industries Ltd introduced a high-purity electrolyte which contained special additives that formed a protective solid electrolyte surface film, the film acts as a layer on graphite preventing serious safety issues and increasing the capacity.

In 2003, the capacity of an 18650 [18 mm diameter and 65mm length] cell reached 2.4Ah with energy density of over 200 Wh/kg due to improved graphite anode materials, electrolyte additives and a stabilized  $\text{LiCoO}_2$ . The capacity reached 2.9Ah using graphite anode, planar Ni based cathode and several different types of additives. MIT researchers Byoungwoo Kang and Gerbrand Ceder have discovered a way to make a lithium iron phosphate ( $\text{LiFePO}_4$ ) battery charge and discharge about as fast as super capacitors. They achieved high capacities like 100 mAh/g at rates as high as 200C.

**Advances in Lithium-ion Battery Technology**

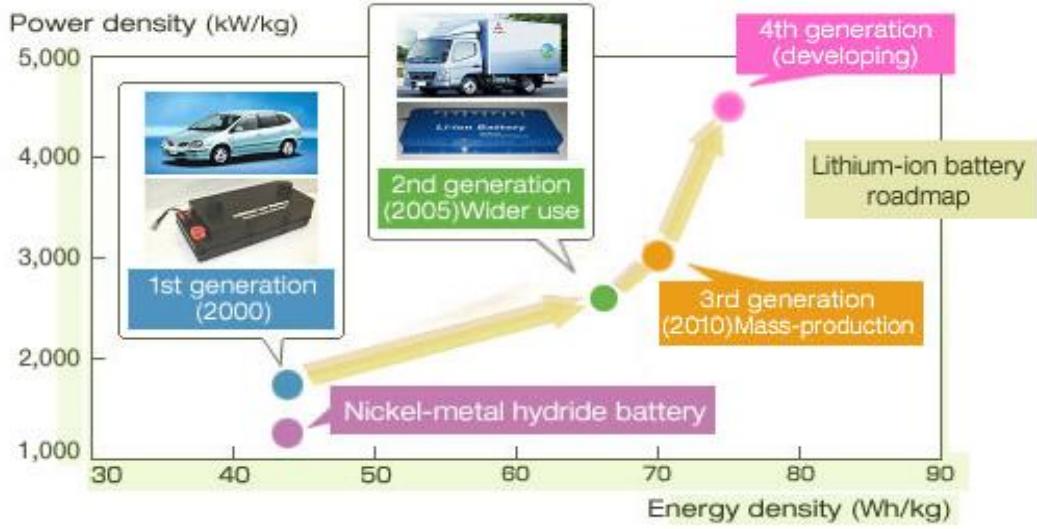


**Figure 3. Advances in Lithium-ion Battery Technology**

*1.4 Lithium ion battery anodes*

Extensive research has been done on improving anode materials in the recent past. Lithium metal is a good anode material because of high theoretical specific capacity but formation of dendrite affects cycleability and raises safety problems. [7]

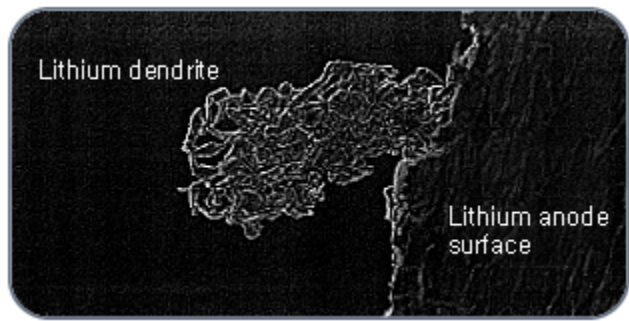


**Figure 4. Dendrite from lithium anode surface by Xeno energy**

During charging, lithium gets deposited on lithium anode and on discharging lithium dendrite cuts from the anode which is called “dead lithium”, this dead lithium starts to accumulate on the anode or float in the electrolyte. This means that active material is consumed and cell life decreases. The other problem with lithium metal anode is the formation of solid electrolyte interface on the electrode which can lead to a loss of capacity, an increased kinetic barrier, poor cycleability and self-discharge. [6]

Graphite was then identified as a potential replacement to lithium metal anode because of its low cost and operational voltage. Graphite is built of ABAB layers held together by van der Waals forces and each layer contains conjugated  $sp^2$  bonds. The carbon anodes are categorized into graphite, hard carbon anodes which does not graphitize even if it is heat treated at higher temperature, soft carbon which easily changes with heat treatment. The intercalation in these “soft carbon anodes” happens through well defined, reversible stages and progressive intercalation within these graphene layers to form  $LiC_6$  with theoretical capacity of 372 mAh/g. The intercalation process happens well below the decomposition limit of common electrolytes. This decomposition tends to form a layer on the carbonaceous anodes; the formation of this film is accompanied by some initial irreversible capacity resulting into the evolution of gas products which is highly undesirable for the battery processability and safety.

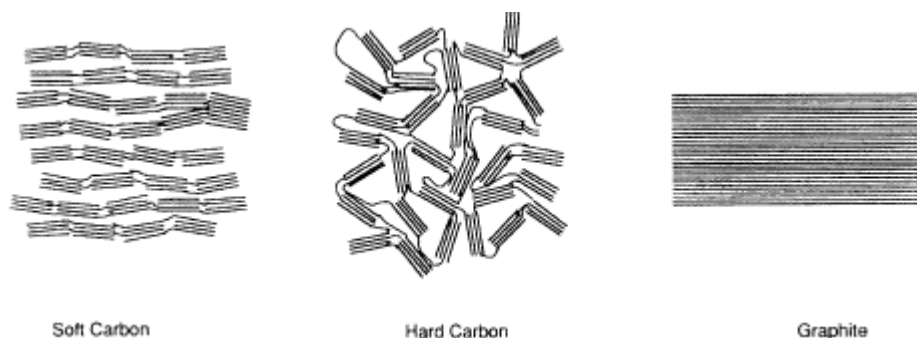


**Figure 5. Difference between structures of Soft carbon, Hard carbon and Graphite**

MesoCarbon MicroBead (MCMB) prepared from petroleum pitch or coal tar is one of the candidate carbon materials available commercially with capacities as high as 500 mAh/g and a spherical structure that easily close pack, results in high density of electrode. Its low surface area can also minimize the side reactions during charge-discharge process.

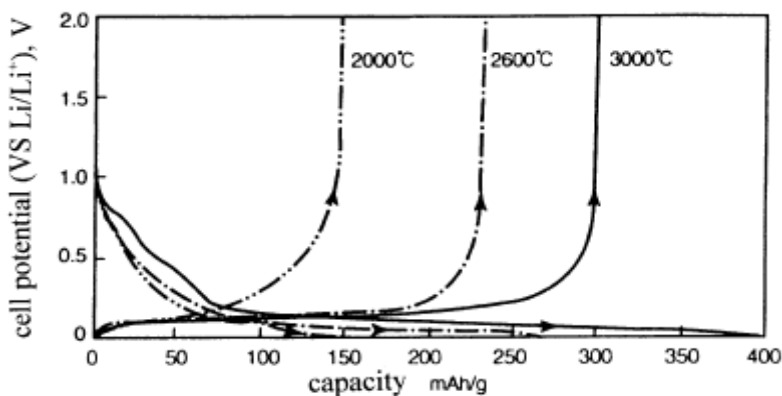


**Figure 6. Charge – discharge curve of MCMB heat treated at various temperatures.**

### 1.5 Electrolytes

Since the mean discharge or charge voltage of Li ion batteries is more than 3V in range, inorganic salts dissolved in organic liquids with large stability window are selected. The desired qualities of a good electrolyte should be good ionic conductivity, high chemical stability, safety

and solvents with low melting point and high melting point are desirable. The ionic conductivity depends on mobility of lithium ions. [8] Carbonic acid esters like ethylene carbonate (EC) have good dielectric constants but high viscosity, which could impair the mobility of ions. A mixture of EC with diethyl carbonate was used in proper molar ratios with a  $\text{LiPF}_6$  salt is a good organic electrolyte.

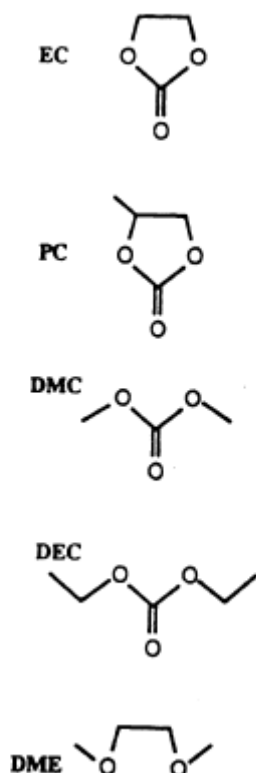


**Figure 7. Structural formulae of main organic solvents [8]**

To further improve safety polymer electrolytes were introduced. The gel type solid polymer electrolyte contains an organic liquid plasticizer. It improves ionic conductivity and safety of the electrolyte. In general, polymer electrolytes have lower conductivity than liquid electrolytes and cannot deliver high power at room temperatures. But polymer electrolytes have advantages like

ease of battery fabrication in various shapes and better safety than conventional organic electrolytes.

### 1.6 Battery Design and Commercialization

The basic cell chemistry and design is similar for all types of Li-ion automotive cells. Thin layers of cathode, separator, and anode are rolled up on a central mandrel and inserted into a cylindrical can. The gaps are filled with liquid electrolyte. The basic design remains unchanged even with change in cathode material, although the layer thicknesses might change. This is the same design used for most small commercial cells, like the 18650.[9]

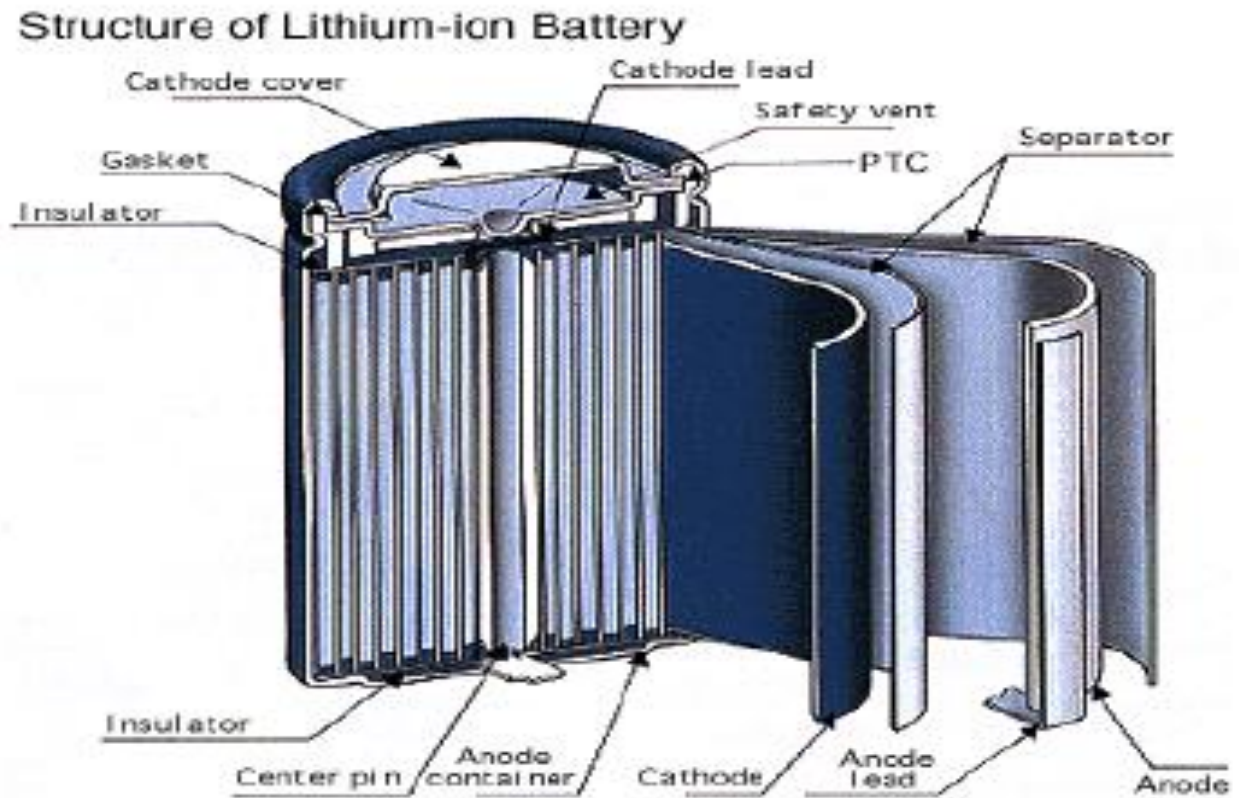
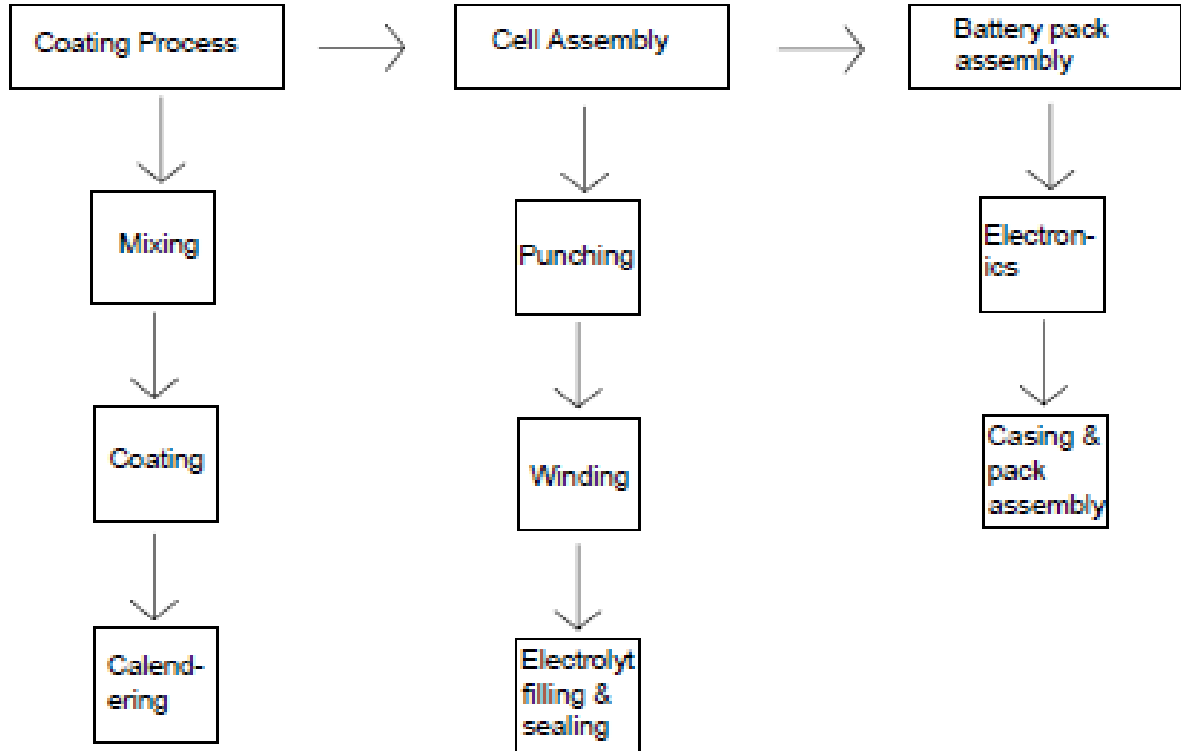


Figure 8. Structure of lithium ion battery[9]

For fabrication of a positive electrode, slurry is prepared from the active material and it is coated on aluminum foil. This slurry generally contains active material, conductive agent such as acetylene black and a binder such as PVDF (Polyvinylidene Fluoride). The slurry of a negative electrode material consists of carbon active material, PVDF as binder and a solvent such as NMP (N -methyl pyrrolidone). Negative electrode uses copper foil as a current conductor for coating. The electrode slurries are uniformly coated onto both sides of the current conducting foils. Proper mixing techniques result in a uniform distribution of the components of the active mass during the coating operation

Coating operations can use slot die, reverse roll coating or doctor blade coating equipment. Coating thickness has to be closely controlled to ensure that all parts fit into the can. After coating, the foil has to be dried before it winds into the can for accurate control of electrode thickness. It is then calendared to increase the yield from winding process.



**Figure 9. Process flow of Lithium ion battery fabrication**

The battery requirements are different for electric vehicles (EV's) and hybrid electric vehicles (HEV's). Typically, electric vehicles need a battery with high energy density to compensate the energy gasoline engine vehicle. These high energy battery packs store about 35 kWh of energy and the cell manufactured for high energy density have energy densities as high as 175 Wh/L.

Fuel is the main source of energy for hybrid vehicles and battery pack is used as a power boost for rapid acceleration. So it needs high power density batteries and cells for this purpose have power densities as high as 2700 W/L.

Both high energy and high power cells have same spiral wound design but there would be change in size of the cell and cell chemistry. High power cell should be smaller than higher

energy cells so as to dissipate higher heat load generated. Moreover, high power cells need less energy than high energy cells, so HEV battery packs are usually smaller than EV packs.

## Chapter 2 Cathode Materials

### 2.1 History of cathode materials

Most of the research in the last two decades has been focused on cathode materials. The theoretical specific capacity of a carbon anode is 372mAh/g. To match that capacity a cathode has to be synthesized having a similar specific capacity and formidable capacity retention. The energy of a battery is the product of its voltage and capacity, a battery with a higher energy density is obtained for a material with a higher voltage and a higher capacity. Therefore, when the same anode material is used, higher voltage and capacity of cathode would give a high energy battery [21]. An ideal cathode material should have excellent power capability, low and stable impedance during battery operation, good thermal safety characteristics, and low cost.

Stanford researchers have discovered layered dichalcogenides like  $\text{TiS}_2$  in the 1970s. It had benefits like a single phase with lithium over the entire composition range but had low ion diffusivity. Later in 1990, layered oxides like  $\text{LiCoO}_2$  came into existence for their ability to release about half lithium atom per mole, and oxidize half of the cobalt to the tetravalent stage, the resulting specific capacity is close to 140 Ah/kg, and capacity density 690 Ah/l.[22]. However,  $\text{LiNiO}_2$  suffers from structural instabilities like nickel ions migrate into lithium sites in the structure leading to reduced lithium diffusivity and storage capacity. In 1996, olivine structured  $\text{LiFePO}_4$  was discovered to replace the layered oxides but it had disadvantages like low electrical conductivity which limits the reversible capacity. These were replaced by solid solutions of layered transition oxides like  $\text{LiCoO}_2 - \text{Li}_2\text{MnO}_3$  and ternary compositions of these oxides. A detailed explanation of layered, spinel and other structure cathodes are given in the following sections.

## 2.2 Olivine and Spinel structure cathodes

Olivine structure cathodes like  $\text{LiFePO}_4$  gained importance with its discovery in 1997 by Padhi et al [23]. It has a theoretical capacity of 170 mAh/g and is environmentally benign, inexpensive, shows excellent cycle stability due to structural similarity between charged/discharged states. Since its discovery many researchers have been trying to improve its performance.

$\text{LiFePO}_4$  can be synthesized by high temperature reactions, sol-gel methods and under hydrothermal conditions. Synthesis under hydrothermal conditions for a short time has proven to be an effective method with good X-ray patterns. But, it gives poor electrochemical properties because of iron atoms blocking the lithium diffusion. This blocking can be stopped by adding reducing agent during synthesis to prevent surface ferric films. The electronic conductivity has been increased from  $10^{-9}$  to  $10^{-5}$  S/cm by coating the material with carbon gel during synthesis and reducing the particle size. However, reducing particle size leads to lower electrode density and lower energy density, and coating process requires too much carbon and these drawbacks prevent it from commercial application.

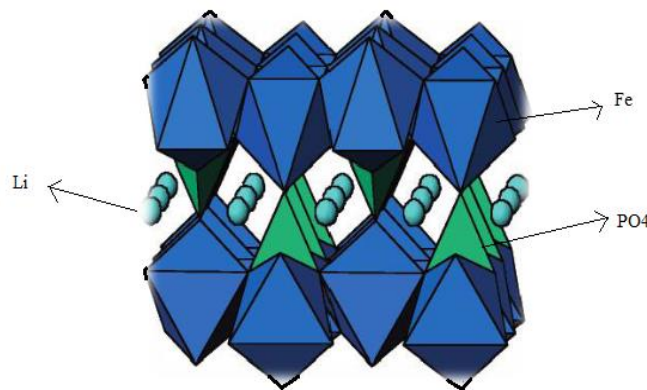


**Figure 10. Olivine structure of  $\text{LiFePO}_4$ .**

The spinel cathode  $\text{LiMn}_2\text{O}_4$  was proposed by Thackeray et.al. and later developed by Bellcore Labs. It has been extensively studied as positive electrode materials of large-size lithium ion batteries for power sources of hybrid electric vehicles because they have several advantages such as lower cost, high-rate capability and higher thermal stability compared to those of Co or Ni based layered materials.  $\text{LiMn}_2\text{O}_4$  is a member of  $\text{AB}_2\text{O}_4$  family of oxides and its structure is spinel. This structure consists of an face-centered cubic (fcc) oxygen packing in which Mn ions occupy the octahedrally coordinated 16d sites while Li ions are located in tetrahedral 8a sites of the  $\text{Fd}\bar{3}\text{m}$  space group.

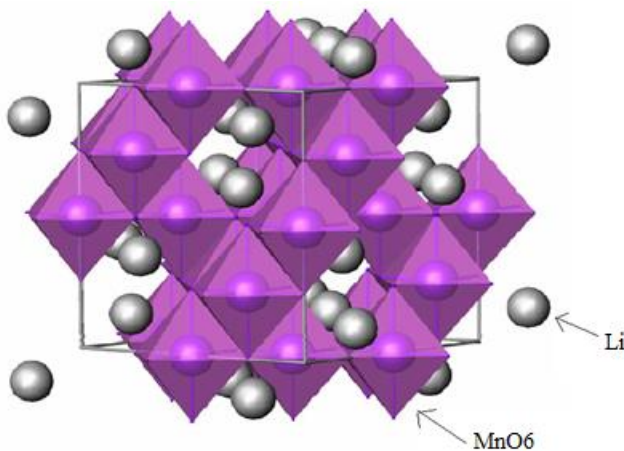


**Figure 11. Spinel structure of  $\text{LiMn}_2\text{O}_4$**

$\text{LiMn}_2\text{O}_4$  has two voltage regions in its cycling curve. One is at 4V range and the other at 3V range with a theoretical capacity of 148 mAh/g. The main problem for the application of Mn spinel is the capacity fading upon cycling which is worst at elevated temperature (above 60C). Many possible sources had been proposed, such as structural instability, Mn dissolution into the electrolyte, the cooperative Jahn-Teller effect. The substitution of foreign metal ions for part of Mn in  $\text{LiMn}_2\text{O}_4$ , such as Li, Ni, Co, Fe, Al can improve its cyclic performance but with increase in capacity fading. This material has been plagued by self-discharge when left under full charge,

particularly at elevated temperatures; this problem may have been solved by switching from the fluoride-containing  $\text{LiPF}_6$  salt which in the presence of traces of moisture can generate HF, to salts such as LiBOB.

## 2.3 Layered Compounds

### 2.3.1 $\text{LiCoO}_2$

A compound having structure similar to layered dichalcogenides was recognized by Goodenough. The first lithium ion battery was commercialized by SONY using carbon as anode and  $\text{LiCoO}_2$  as cathode. Now, most of the commercial lithium ion batteries are built with  $\text{LiCoO}_2$ . It has the  $\alpha\text{-NaFeO}_2$  structure with oxygen in a cubic close-packed arrangement. On complete removal of the lithium, the oxygen layers rearrange themselves to give hexagonal close packing of the oxygen in  $\text{CoO}_2$ .

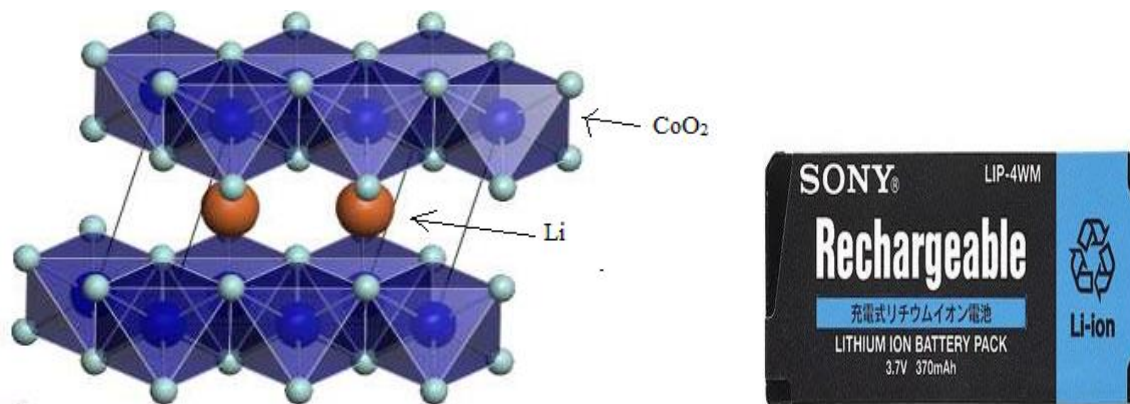


**Figure 12. Structure of  $\text{LiCoO}_2$  and the SONY commercial battery**

The capacity is around 130 mAh/g because around 0.5 Li/Co only can be cycled without causing capacity loss during cycling. Synthesis at lower temperatures results in disorder distribution of ions forming spinel phase having low electrochemical and cycling properties. The cathode also

undergoes phase transformation from hexagonal to monoclinic when charged above 4.2V results in practical capacity which is half the theoretical capacity. This phase transformation is proved to be suppressed by substitution of foreign ions such as Li, Mg, Al, Fe, Ni, Cr and Mn instead of some Co ions in  $\text{LiCoO}_2$ . The effect of these foreign elements on its electrochemical behavior depends upon the nature of substituents. If elements which are electrochemically inert like Al are substituted, it increases the de-intercalation voltage. Substitution of Ni and Cr might decrease the voltage. Modification of  $\text{LiCoO}_2$  surface with metal oxides such as  $\text{Al}_2\text{O}_3$  increases the cycleability of the cathode material; the mechanism for the protection is related to minimizing the reactivity of  $\text{Co}^{4+}$  charge with HF formed when electrolyte salt  $\text{LiPF}_6$  reacts with moisture. Solid solutions with other compounds like  $\text{LiCoO}_2\text{-Li}_2\text{MnO}_3$ ,  $\text{LiCoO}_2\text{-LiNiO}_2$ ,  $\text{LiNi}_{0.5}\text{Mn}_{0.5}\text{O}_2$ - $\text{LiCoO}_2\text{-Li}_2\text{MnO}_3$  are also reported to improve the capacity retention.

Although  $\text{LiCoO}_2$  dominates the li ion battery industry, it has drawbacks like cost and toxicity. The amount of Co content is limited, which increases the cost of the cell. This limits the cathode to be used for various applications. Since the cost and toxicity of Ni, Mn, Fe, and Ti are lower than that of Co, compounds based on these elements are extensively investigated as alternatives to  $\text{LiCoO}_2$ .

### 2.3.2 $\text{Li}_2\text{MnO}_3$

Lithium intercalation compounds based on manganese oxides are cheaper and less toxic than  $\text{LiCoO}_2$ . As a result  $\text{Li}_2\text{MnO}_3$  represented as  $\text{Li}[\text{Li}_{1/3}\text{Mn}_{2/3}]\text{O}_2$  gained importance in the recent years. It has a layered rock salt phase structure. Lithium de-intercalation occurs by oxidation of  $\text{Mn}^{+3}$  to  $\text{Mn}^{+4}$ , but it is impossible to attain  $\text{Mn}^{+5}$  state in oxygen environment. An alternative mechanism proposed for electrochemical extraction of  $\text{Li}^+$  from oxides containing  $\text{Mn}^{4+}$ ,

involves the simultaneous removal of  $O^{2-}$ . This mechanism provides additional lithium for extraction giving out higher voltages on the first charge. It is free from complications that might occur due to mixed transitional metal oxides, being a layered compound Li ions are mobile in the alkali metal layers and their removal is limited only by the ease of oxidizing tetravalent Mn. It was also shown that dominant process was exchange of  $Li^+$  by  $H^+$  at low proton concentrations, whereas oxygen loss accompanied exchange at high  $H^+$  concentrations.

The structure of  $Li_2MnO_3$  consists of cubic close-packed oxide ions with alternate sheets of octahedral sites between the close packed layers occupied by Li and  $[Li_{1/3}Mn_{2/3}]$ . If the lithium and manganese ions in the transition metal layers are disordered then the structure is that of a simple layered compound with space group  $R\bar{3}m$ .

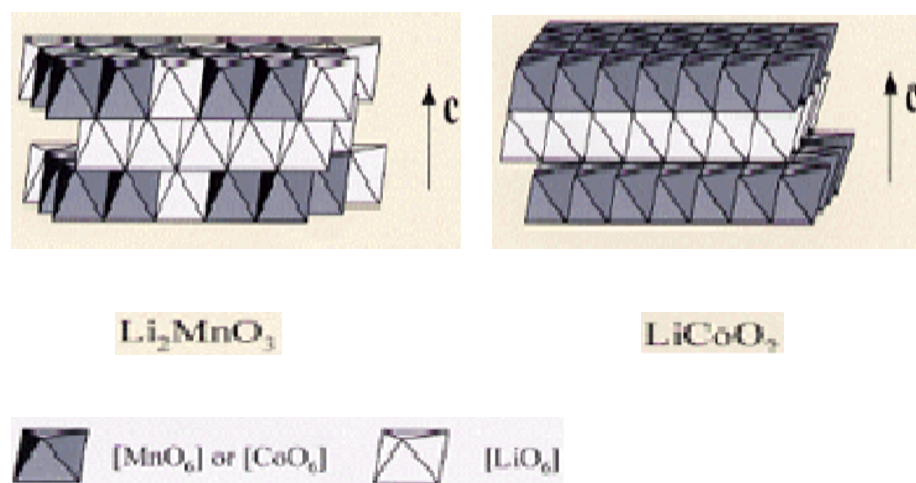


**Figure 13. Comparison of  $Li_2MnO_3$  and  $LiCoO_2$  structures**

The  $Li_2MnO_3$  synthesized using different starting materials and calcination temperatures show different structural properties, surface morphologies, and electrochemical reversible capacities. Layers rich in  $Li_2CO_3$  and  $LiOH$  are formed on the surfaces of transitional metal oxides before their interaction with the electrolyte, this layer for depletes when it comes in contact with the

non-aqueous electrolyte. Solid solutions of  $\text{Li}_2\text{MnO}_3$  with other materials show that it produces large ICL but also exhibits good cycleability decreasing the capacity fading of  $\text{LiCoO}_2$  solution.

### 2.3.3 $\text{LiNi}_{0.8}\text{Co}_{0.15}\text{Al}_{0.05}\text{O}_2$

High power lithium ion cells were developed by Argonne national laboratory as a part of the U.S. Department of Energy's Advanced Technology Development Program (ATD). These cells contain the cathode  $\text{LiNi}_{0.8}\text{Co}_{0.15}\text{Al}_{0.05}\text{O}_2$  which is called Gen 2 material, graphite-based anodes and  $\text{LiPF}_6$ -based electrolytes initially meet the low-impedance criteria required to meet the high-power requirements for hybrid electric vehicle applications.

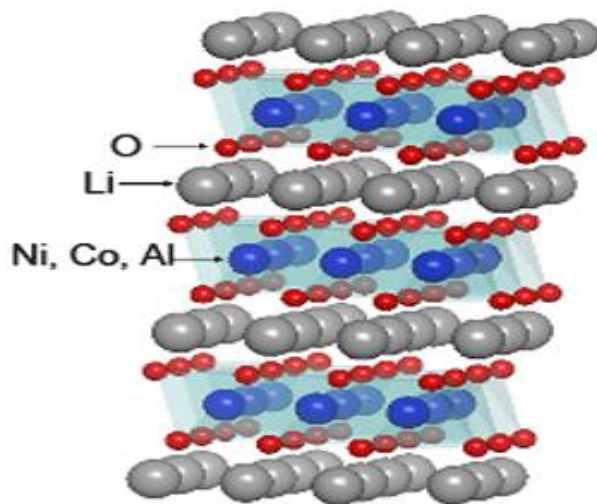


**Figure 14. Structure of  $\text{LiNi}_{0.8}\text{Co}_{0.15}\text{Al}_{0.05}\text{O}_2$**

It is an isostructural compound of  $\text{LiCoO}_2$  with rhombohedral crystal system and R-3m space group. The material is produced in the ultrafine particle form, which has high reactivity while maintaining the highly ordered layered structure. The high nickel content usually gives higher initial specific capacity while cobalt and aluminum improve the structural stability and life cycle.

It is considered to have better thermal stability than  $\text{LiNiO}_2$ , as the H3 phase peak of  $\text{LiNiO}_2$  which contributes for thermal instability is suppressed in the case of  $\text{LiNi}_{0.8}\text{Co}_{0.15}\text{Al}_{0.05}\text{O}_2$ . In this type of cathode material, the specific capacity is affected by  $\text{Li}^+/\text{Ni}^{3+}$  cation mixing in the crystal structure, which results in lower Li-ion intercalation capacity. Due to this mixing, some of the tetrahedral positions are occupied by  $\text{Ni}^{3+}$  and thus are not available for Li-ion intercalation. The percentage of Li/Ni ion mixing can be determined by Rietveld refinement on powder XRD.

The grain size can be from 250nm to 30 $\mu\text{m}$  depending on the application with the specific area in the range of 0.30-2.0  $\text{m}^2/\text{g}$ . The ultrafine grain size and high surface area gives higher rate capability and higher utilization. This grain size also helps to increase the active sites for lithium ion intercalation and reduces the diffusion distance in the active material which allows it work well at higher rates. The highly ordered crystal structure of the cathode material allows it to remain stable after extended cycles. The initial crystal structure of the cathode material not only determines the initial specific capacity, but also determines the stability after extended cycling. The stability of delithiated cathode is important to increase the cycle life. After the lithium-ion comes out, Ni or Co will be oxidized from +3 to +4 valence state, the crystal cell undergoes volume change. Aluminum remains in the +3 valence state, and has no contribution to the capacity but it helps to reduce the crystal volume change and keep the structure stable after cycling.

On accelerated aging, capacity decreases and cell impedance increases. According to the electrochemical measurements, it not only contributes to impedance raise but also capacity fade at 1C which was due to formation of surface film between the electrode and the electrolyte. Two mechanisms have been reported for the formation of the surface film. First one is that the ring-opening of the ethylene carbonate molecule present in the electrolyte by  $\text{PF}_5$  in the salt produces

oligomers in the electrolyte that coat the electrode surfaces. These oligomers may cross-link adjacent to the positive electrode at high-electrode voltages, producing barriers that impede the motion of lithium-ions increasing the cell impedance. Release of Oxygen from the cathode into the electrolyte causing a reaction to occur is considered to be the second mechanism.

#### 2.4 Solid solutions and ternary compositions

Solid solutions and ternary compositions have been made to increase structural stability, capacity retention, reduce the costs and increase the initial specific capacity. With increase in demand for advanced lithium ion batteries, complicated compositional cathode material were given importance. These complicated compounds have retained the advantages of their single transition metal species and overcome their shortcomings, which has extended the research fields of the cathode materials for lithium ion batteries.  $\text{LiNi}_{1-x}\text{Co}_x\text{O}_2$ , a solid solution of  $\text{LiCoO}_2$  and  $\text{LiNiO}_2$  was the first reported solution. It has better capacity, thermal stability, and capacity retention with reduced costs because of low Co content when compared to its base compounds  $\text{LiCoO}_2$  and  $\text{LiNiO}_2$ . Many solid solutions like  $\text{LiCrO}_2\text{-Li}_2\text{MnO}_3$ ,  $\text{LiNiO}_2\text{-Li}_2\text{MnO}_3$ ,  $\text{LiNi}_{0.5}\text{Mn}_{0.5}\text{O}_2\text{-Li}_2\text{MnO}_3$ ,  $\text{Li}_2\text{MnO}_3\text{-LiNi}_{1-x}\text{Co}_x\text{O}_2$ ,  $\text{Li}_2\text{MnO}_3\text{-LiCoO}_2$ ,  $\text{LiFeO}_2\text{-Li}_2\text{MnO}_3$ ,  $\text{LiNi}_{0.5}\text{Mn}_{0.5}\text{O}_2\text{-Li}_2\text{TiO}_3$  have been made till now. Significant changes were made in improving the layered two-dimensional materials by the Ozhuku, Dahn, Kanno, Zhecheva and Stoyanova groups.

Stoyanova *et al.*[24] reported the effect of manganese substitution for cobalt in solid solution  $\text{Li}_2\text{MnO}_3\text{-LiCoO}_2$  which led to the development of composite-type cathodes. Solid solutions between  $\text{LiMO}_2$  ( $M = \text{Cr}$ ) and  $\text{Li}_2\text{MnO}_3$  layered materials with superior electrochemical performance were demonstrated by Dahn and other groups. A new series of material with the general formula  $x\text{Li}_2\text{MO}_3 \cdot (1 - x)\text{LiMn}_{0.5}\text{Ni}_{0.5}\text{O}_2$  ( $M = \text{Ti, Mn, Zr}$ ) for  $x = 0$  to  $0.3$  was reported.

Approaches to prevent the conversion of layered LiMnO<sub>2</sub> to spinel were explored which led to subsequent improvements of the material. Layered compositions representing solid solution between Li<sub>2</sub>MnO<sub>3</sub>, i.e., Li[Li<sub>1/3</sub>Mn<sub>2/3</sub>]O<sub>2</sub> and LiMn<sub>0.5</sub>Ni<sub>0.5</sub>O<sub>2</sub>, were shown to exhibit high capacities. The new series of cathodes representing a solid solution between layered Li<sub>2</sub>MnO<sub>3</sub> • Li[Li<sub>1-x</sub>Mn<sub>(2-x)/3</sub>Ni<sub>x/3</sub>Co<sub>x/3</sub>]O<sub>2</sub> was proposed by Manthiram et al.[19] which resulted in a high capacity of 285 mAh/g with low irreversible capacity loss.

The solid solution Li<sub>2</sub>MnO<sub>3</sub>-LiCoO<sub>2</sub> made by Sun et,al is discussed. It is believed that valence values of Mn and Co are 4+ and 3+ in the solution. The samples prepared can be indexed as  $\alpha$ -NaFeO<sub>2</sub> structure with R<sub>3m</sub> space confirming its layered structure with super lattices of Li<sub>2</sub>MnO<sub>3</sub>. The charge capacity at the flat high charge plateau is caused by the Li<sub>2</sub>O removal from solid solutions Li<sub>2</sub>MnO<sub>3</sub>-LiCoO<sub>2</sub>. Electrochemical measurements show that the discharge capacity of the samples gradually reduces with the increasing of Li<sub>2</sub>MnO<sub>3</sub> content and the excellent electrochemical cycling performance can be obtained when it is charged to 4.5V. The reason for obtaining high specific capacity at higher rates was because of maintaining layered structure at all times. This solid solution is represented as  $x\text{Li}_2\text{MnO}_3 \cdot (1-x)\text{LiMO}_2$  by Thackeray et,al where M = Co, Ni, Mn.

## Chapter 3 Experimental Methods

Building and testing an electrochemical cell involves material synthesis, characterization, half-cell assembly, cell assembly and electrochemical testing. Material Synthesis was done using the sol-gel method. The following section explains the solid state method and compares it to the sol-gel method. This comparison shows the advantages of sol-gel over solid state synthesis, which was used in this research.

### *3.1 Solid State Synthesis*

Solid State Synthesis has several disadvantages like inhomogeneity, irregular morphology, larger particle size with broader particle size distribution, poor control of stoichiometry, and longer periods of calcination followed by extended grinding. In order to achieve the efficient Lithium utilization at higher rates of charge–discharge, it is necessary to obtain submicron sized particles with a uniform morphology, narrow size distribution, and homogeneity. Sol-gel synthesis needs lower calcination temperatures than solid state synthesis for the formation of desired phase. It also has advantages such as good stoichiometric control, production of submicron-sized particles with narrow particle-size distribution and relatively shorter processing time.[13] The sol–gel process can undergo polyesterification when heated in a poly hydroxyl alcohol to form a solid polymeric resin throughout which the cations are uniformly distributed. Thus, the resin retains homogeneity on the atomic scale and fine particulate oxides may be yielded through calcination at low temperature.[14]

### 3.2 Sol-gel Synthesis

The terminology “sol–gel” is used to describe the process in which a solid phase is formed through gelation of a solution. Drying of the gel can then give the dry gel state and subsequent heat treatment can be used to remove unreacted organic residues, stabilize the gel and for crystallization [18].

Sol-gel synthesis was used to make all the samples. This method requires a lower calcination temperature than solid state synthesis [10]. Acetates  $\text{Li}(\text{COOCH}_3)_2 \cdot 2\text{H}_2\text{O}$ ,  $\text{Mn}(\text{COOCH}_3)_2 \cdot 4\text{H}_2\text{O}$ ,  $\text{Ni}(\text{COOCH}_3)_2 \cdot 4\text{H}_2\text{O}$ ,  $\text{Co}(\text{COOCH}_3)_2 \cdot 4\text{H}_2\text{O}$  and nitrate  $\text{Al}(\text{NO}_3)_3 \cdot 9\text{H}_2\text{O}$  were used as precursor agents.

Stoichiometric amounts of acetates and nitrate were measured and a batch size of five grams was considered. These precursors were dissolved in de-ionized water and an equi-molar amount of citric acid was added under constant stirring. Citric acid acts as a chelating agent which helps in pyrolysis of the gel precursor and accelerates the decomposition of acetate ions. Decomposed acetate ions act as oxidizer and help the gel in burning. The solution was stirred at  $100^\circ\text{C}$  until a gel was obtained. It was then calcined at  $300^\circ\text{C}$  for 3 hours. This first heating helps in decomposition of organic compounds by burning off the acetates. However, it is difficult to attain the desired phase and crystalline structure is in this first heating. Thus, the powders were ground and subjected to second heating at  $800^\circ\text{C}$  for 10 hours [11] and then subjected to furnace cooling. Zhang et al used  $950\text{--}1000^\circ\text{C}$  as second heating temperature for similar precursors [12]. The reason for using lower temperatures is the type of synthesis. Sol-gel synthesis requires lower temperatures than solid state synthesis. The temperature was chosen high enough for proper

phase formation but not so high that it results in undesired decompositions. The material was collected from furnace, ground and stored in a vacuum oven until the cathode preparation.

### 3.3 Characterization

#### 3.3.1 X-ray diffraction

X-ray diffraction (XRD) analysis investigates crystalline material structure, atomic arrangement, crystallite size and imperfections. Every crystalline substance gives a unique pattern; in a mixture of crystalline phases each phase produces patterns that are different from others. This pattern is like finger print of a substance suitable for characterization of polycrystalline phases. Today about 50,000 inorganic and 25,000 organic single components, crystalline phases, and diffraction patterns have been collected and stored as standards.

Bragg's law governs the diffraction analysis. When X-rays are scattered from a crystal lattice, the observed peak intensity corresponds to path difference equal to integral number of wavelengths. A scattered wave is represented below.

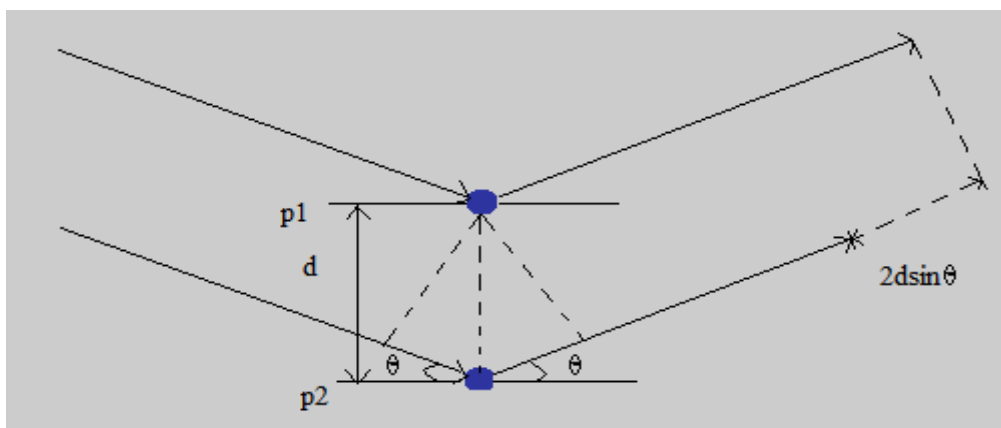


**Figure 15. Working of XRD**

Where  $n$  is the order,  $d$  is the lattice spacing,  $\lambda$  is the wavelength of X-rays and  $\theta$  is the angle between the incident ray and the plane of the material. The condition for maximum intensity in the Bragg's law allows us to determine the crystal structure or the wavelength of X-rays incident upon the crystal. The scattered wave is strong if it satisfies

$$n\lambda = 2d\sin\theta$$

All samples were characterized using a Scintag X2 Advanced diffractometer with Cu  $K\alpha$  radiation and a Peltier detector with stationary sample stage. The Scintag X2 is extremely useful for qualitative and quantitative analysis of powder samples.

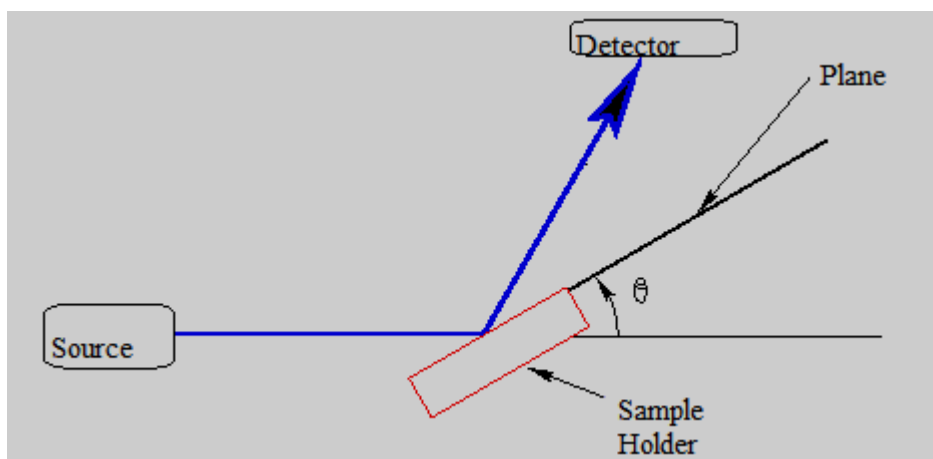


**Figure 16. Schematic representation of Scintag Diffractometer**

All the samples were in powder form and were scanned from  $2\theta$  values of 15 to  $70^\circ$  at a rate of  $5^\circ$  per minute. Promising samples were chosen from the results of electrochemical tests and Rietveld Refinement was performed on them for better characterization of the materials. Scans on the Scintag were done at room temperature in the ambient environment.

### 3.3.2 Differential Scanning Calorimeter

The Differential scanning calorimeter (DSC) is a thermal analysis instrument that determines the temperature and heat flow associated with material transitions as a function of time and temperature. The DSC can be used to determine the glass transition, melting temperature and freezing temperatures, first order phase transition heat of fusion, percent crystallinity, crystallization kinetics and phase transitions, oxidative stability and curing kinetics. The components of a DSC are the furnace (where heating and reference pans are maintained at desired temperature region), the auto sampler (which loads and unloads the pans according to the commands), the cooling system (which cools the sample and keeps it in the desired temperature region) and computer (interface between user and the instrument).

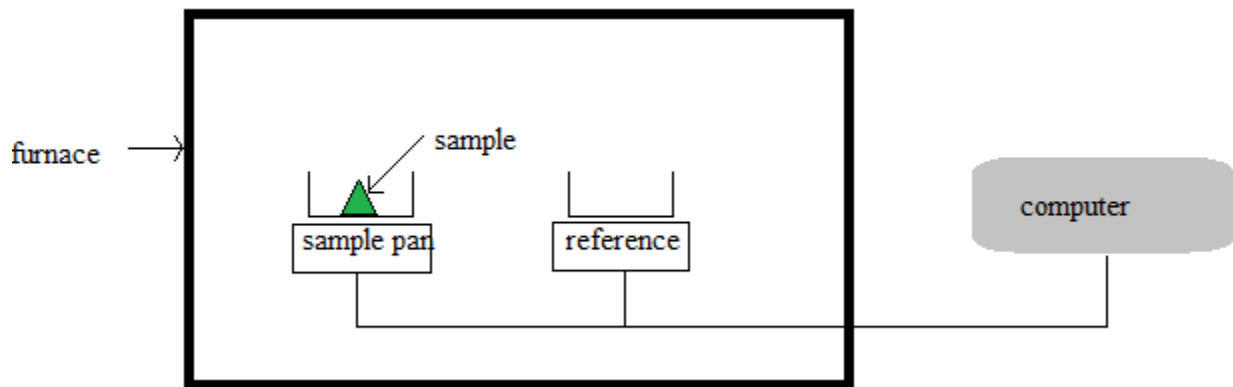


**Figure 17. Schematic representation of the Differential scanning calorimeter (DSC)**

There are two pans, one of them is the reference pan and the other has sample in it. The computer is then programmed to heat the pans at the same time. The heating rate differs with

material present in the sample pan. Heat flow with reference to the temperature is plotted. The melting of the sample is usually considered for analysis. When heat is supplied to the sample, at a definite temperature crystalline material starts melting. At this temperature it absorbs more heat in order to melt the crystals and also keep the temperature rising at the same rate as the reference pan. This extra heat shows up as a peak on the DSC curve. DSC curves of  $\text{LiNiO}_2$  and  $\text{LiCoO}_2$  are shown below for better understanding.

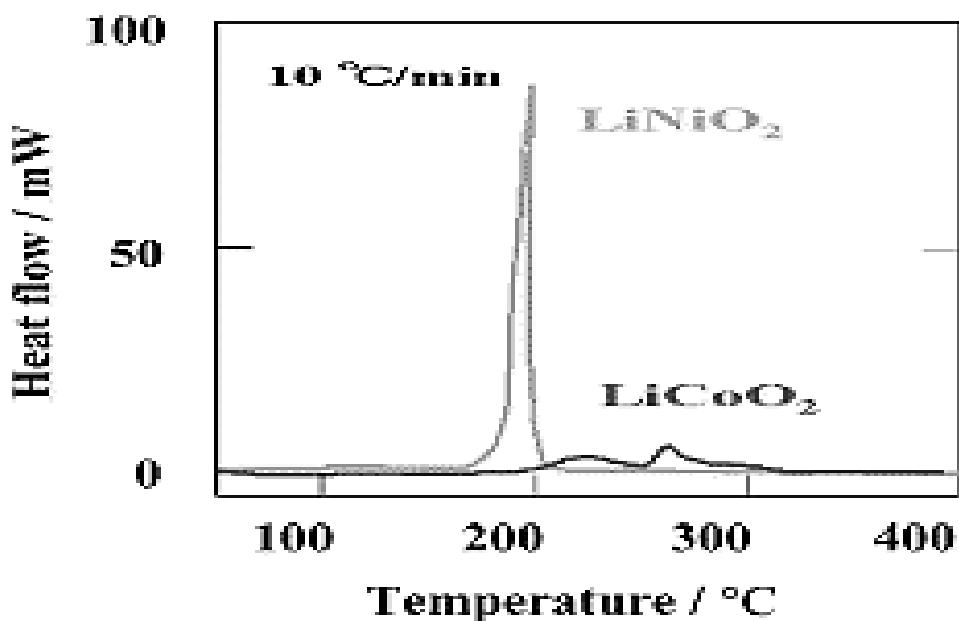


**Figure 18. Example of a DSC curve**

The apparatus available was a Modulated Differential Scanning Calorimeter with liquid nitrogen accessory (DSC 2920) made by TA instruments

### 3.3.3 ICP/AES

ICP/AES is a type of analytical atomic spectroscopy that uses plasma as the atomization and excitation source. The sample is dissolved in a liquid and that liquid is converted into an aerosol. Water is driven off, and remaining solid and liquid portions are converted to gases. It is subjected to atomization resulting in breaking of gas phase bonds. Atoms gain energy from collisions and emit light of characteristic wavelength which is quantitatively measured.[17]

The instrument used for the samples was a Perkin Elmer Optima 7300 DV with a Cetac ASX-520 auto sampler. It contains Meinhard concentric nebulizer and cyclonic spray chamber with baffle.



**Figure 19. Perkin Elmer Optima 7300 DV with a Cetac ASX-520 auto sampler**

### *3.4 Half Cell Assembly*

After sol-gel synthesis, the material was ground to fine powder and then sieved through 45 $\mu$ m sieves to obtain an optimal size for all the particles. For making disc electrodes, 75% active material was mixed with 20% acetylene black and 5% polytetrafluoroethylene (PTFE). The active material and acetylene black was ball milled together for 20 minutes using an 8000M mixer and water suspended PTFE drops were added and the material was dried for 12 hours in the oven.

The material was then rolled out into thin sheets using a roller. A punch was used on those sheets to obtain a coin cell of a half-inch diameter. This punching was repeated until the desired weight was obtained. The weights of the cathodes were maintained from 0.021 to 0.029 gms. The thickness obtained for these weights would be approximately 50-60  $\mu$ m. Finished cathodes were stored inside a dry oven until half cells were made from those cathodes.

Half cells were made from those coin cell cathodes before moving them into argon box. These cathodes were placed over an aluminum cylinder; a Whatman Glass microfiber filter with a pore size of 0.7 $\mu$ m was placed on the top to separate the cathode from electrolyte. A separator made up of porous polypropylene sheet called Cell Guard 2400 was placed on the filter. A plastic 'T' shaped body was put on cathode side of the cylinder and it was tightened, using a nut to make it air tight.

The electrochemical tests were made using these 'T' cells. These have lower ion diffusivity and electrical conductivity than the cells that are tested by coating the material on the aluminum foil. However, this method is widely used because for its simplicity and the reduced amounts of material used for cathode preparation. 'T' cells were stored in an oven until they were moved

into the argon chamber. Full cells were made inside the argon chamber to maintain the inert atmosphere which is needed for the electrolyte and the anode.

### *3.5 Full Cell Assembly*

Half cells made from the cathode were moved into the argon box. Lithium metal was used as the anode and 1M LiPF<sub>6</sub> salt in a 1:1 volume ratio of ethylene carbonate and dimethyl carbonate was used for the electrolyte. The anode was punched from a lithium metal foil to obtain disks of almost half-inch diameter. It was then placed on the steel cylinder with spring in the middle of the assembly. The spring maintains the electrical conductivity and keeps all the components in contact with each other.

This steel cylinder with springs, separator and anode were inserted into the open side of the ‘T’ cell. It was then sealed using a nut. Electrolyte is added from the top until the electrodes are completely soaked with it and then the top side is also sealed. Once the cells were assembled, they were left in the glove box for 24 hours to ensure diffusion of electrolyte into porous cathode. The following figure 18 shows the full cell assembly.

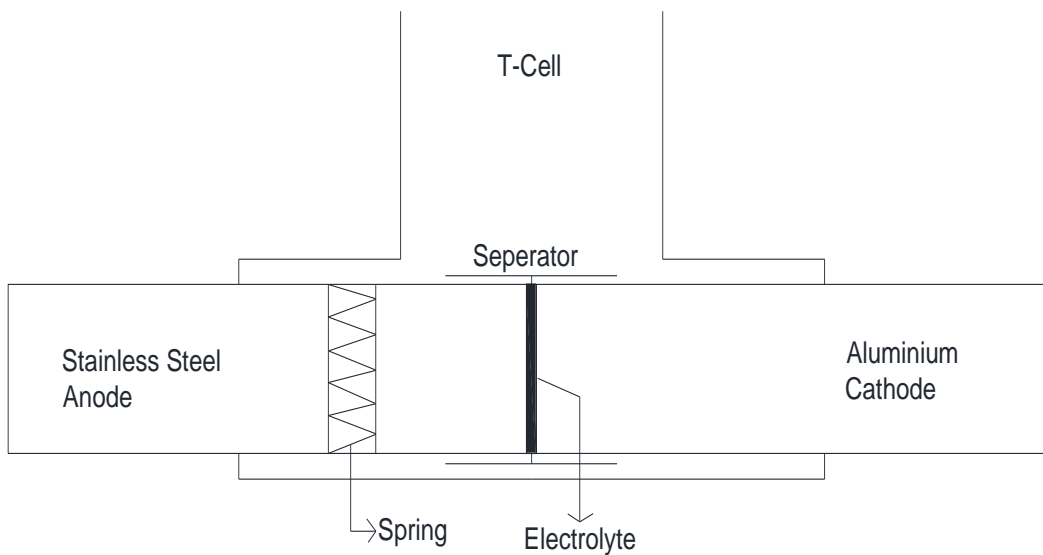


**Figure 20. Representation of a Full Cell Assembly**

### *3.6 Electrochemical Testing*

All the samples were tested with the Arbin BT 2000 battery testing system or cycler. They were cycled between 2V and 4.6V, a constant current of  $300\mu\text{A}$  was supplied. A C-rate of C/15 was maintained for all the cells. A minimum of 4 cycles were performed for all the cells to analyze the cycleability of the sample. The voltage and current are programmed using MITS software available in the computer attached to cycler.

## Chapter 4 OBJECTIVES, APPROACH AND SCOPE

### *4.1 Thesis Statement*

There are cathode compositions in the system  $(1-x-y) \text{LiNi}_{0.8}\text{Co}_{0.15}\text{Al}_{0.05}\text{O}_2 \cdot x\text{Li}_2\text{MnO}_3 \cdot y\text{LiCoO}_2$  that when tested for discharge capacities and cyclability will show better properties than the current generation lithium ion cathode materials.

### *4.2 Objectives*

The objective of the thesis is to find a material composition that has better cyclability and lower cost than the standard battery materials. A ternary composition with low cost materials like Al, Mn and Ni were used instead of Co to reduce the cost of the battery. Some compositions in the system are already recognized to be lower cost and have better properties than  $\text{LiCoO}_2$ . For example,  $\text{LiNi}_{0.8}\text{Co}_{0.15}\text{Al}_{0.05}\text{O}_2$  was reported to have improved safety and cyclability by SAFT and other researchers. This material was assigned as Gen 2 material under Advanced Technology Development Program (ATD). Addition of this material into the system resulted in better cyclability and lower cost. A promising commercial lithium ion battery material was synthesized from this system.

### 4.3 Approach

Solid solutions like  $\text{LiNiO}_2\text{-Li}_2\text{MnO}_3$ ,  $\text{LiCoO}_2\text{-LiNiO}_2\text{-Li}_2\text{MnO}_3$ ,  $\text{LiNi}_{0.5}\text{Mn}_{0.5}\text{O}_2\text{-Li}_2\text{MnO}_3$ ,  $\text{Li}_2\text{MnO}_3\text{-LiNi}_{1-x}\text{Co}_x\text{O}_2$ ,  $\text{Li}_2\text{MnO}_3\text{-LiCoO}_2$ ,  $\text{LiNi}_{0.5}\text{Mn}_{0.5}\text{O}_2\text{-Li}_2\text{MnO}_3\text{-LiCoO}_2$  and  $\text{LiCoO}_2\text{-Li}_2\text{MnO}_3$  have been successfully made into promising cathode materials. Manthiram et al [19] showed a new series of cathode materials represented by  $\text{Li}[\text{Li}_{(1-x)/3}\text{Mn}_{(2-x)/3}\text{Ni}_{x/3}\text{Co}_{x/3}]\text{O}_2$  which is a solid solution between  $\text{Li}_2\text{MnO}_3\text{-Li}[\text{Ni}_{1/3}\text{Mn}_{1/3}\text{Co}_{1/3}]\text{O}_2$ . Zhang et al [12] developed ternary composition with  $(1-x-y)\text{LiNi}_{1/2}\text{Mn}_{1/2}\text{O}_2\text{-xLi}_2\text{MnO}_3\text{-yLiCoO}_2$  system.

Similar methodology of a ternary composition is used to explore novel cathode materials with two-dimensional layered structure by-building ternary composition diagram between iso-structural materials.  $\text{Li}_2\text{MnO}_3$  which can be represented as  $\text{Li}[\text{Li}_{1/3}\text{Mn}_{2/3}]\text{O}_2$  has the same structure as  $\text{LiCoO}_2$ , but there is super-lattice ordering of  $\text{Li}^+$  and  $\text{Mn}^{4+}$  in transition metal layers.  $\text{LiNi}_{0.8}\text{Co}_{0.15}\text{Al}_{0.05}\text{O}_2$  with layered structure, which can be considered as solid solution between  $\text{LiNiO}_2$  and  $\text{LiCoO}_2$  with Al substitution in Co site, is a promising cathode material because of its improved stability, improved electrochemical performance, due to simultaneous Al and Co substitution for Ni in  $\text{LiNiO}_2$ . The improved performance of this material was attributed to structural integrity (the rhombohedral crystal structure phase remains unchanged during repeated charge/discharge cycling). The following figure 19 shows the ternary composition and the points, which are evenly placed across the entire compositional space chosen for synthesis. A total of 28 samples were initially made with the compositions of the 28 points.

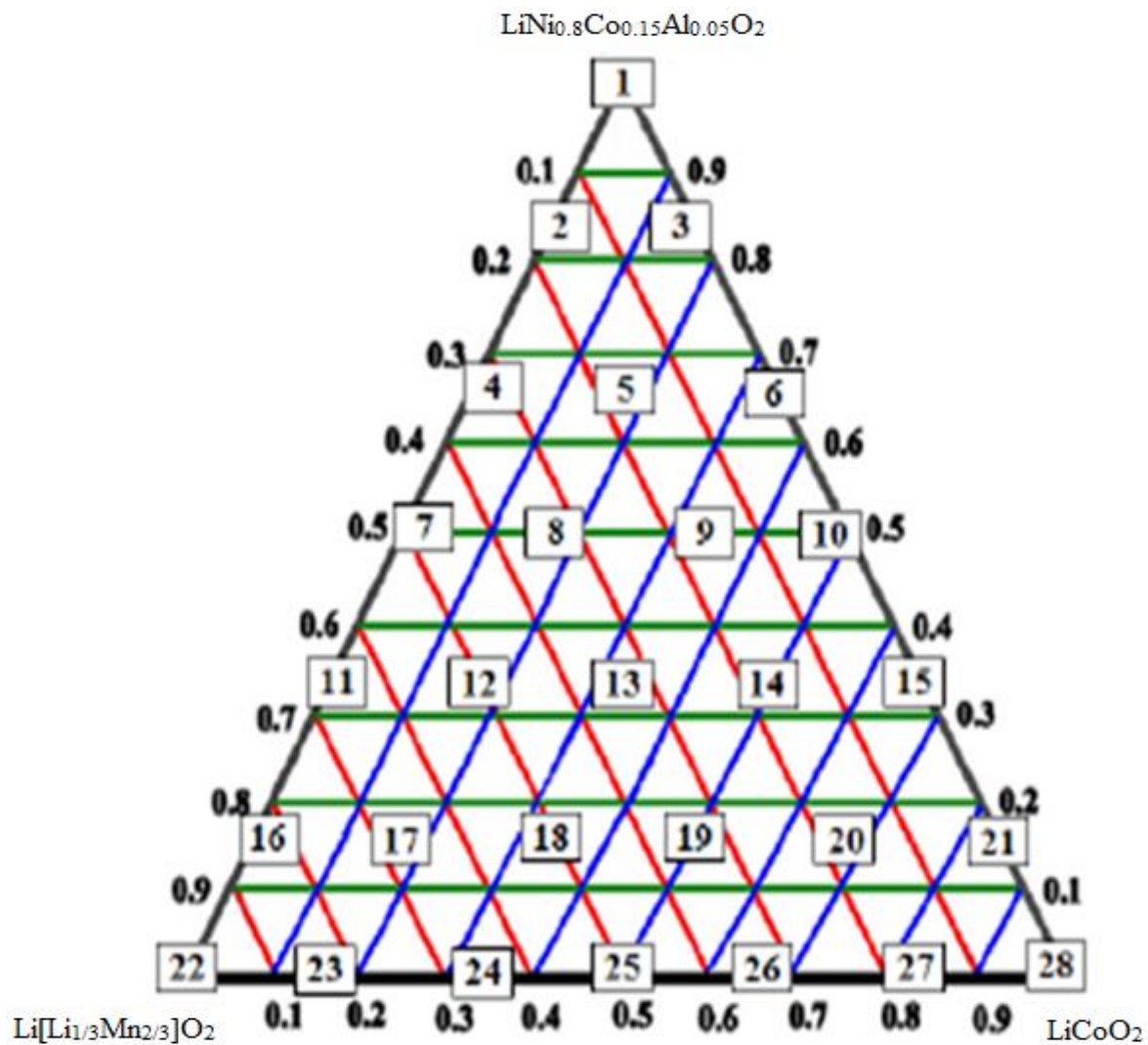


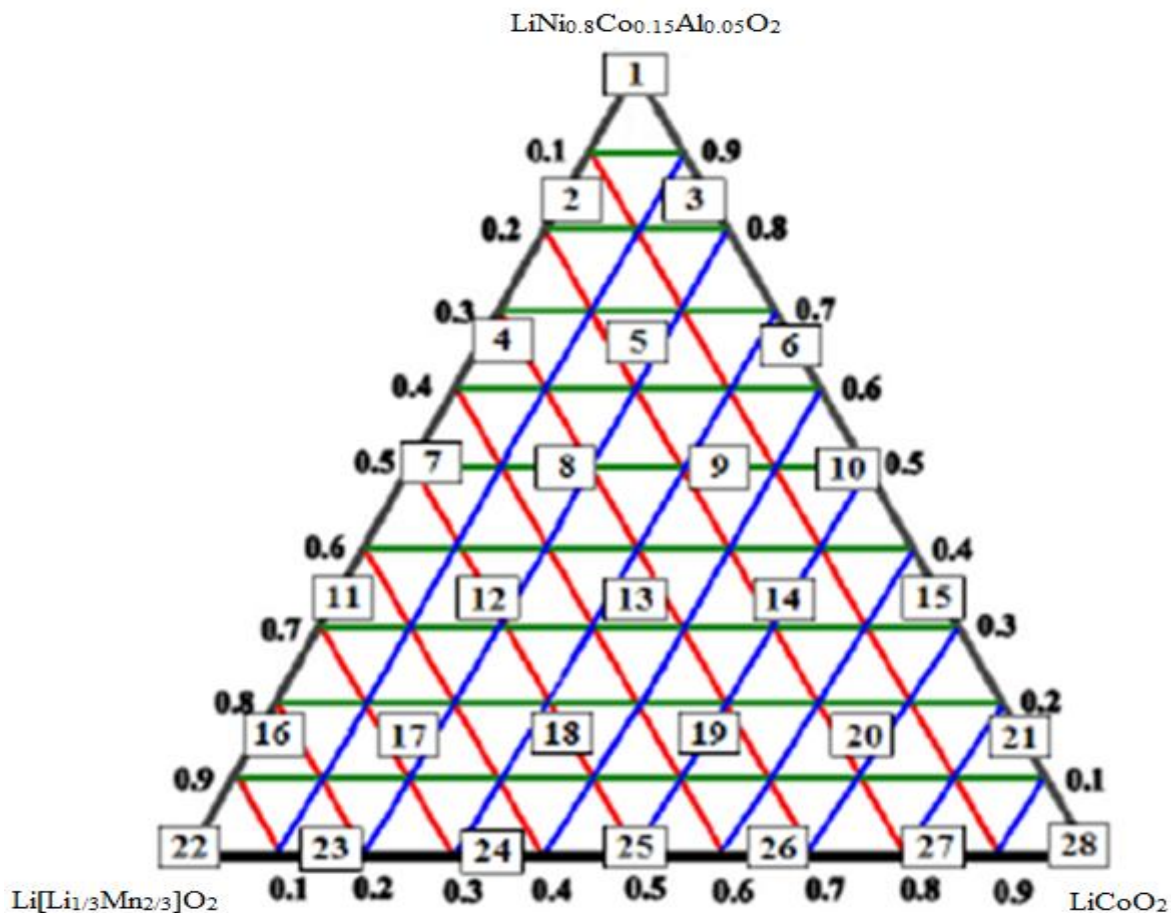
**Figure 21.** Ternary composition of the system  $(1-x-y) \text{LiNi}_{0.8}\text{Co}_{0.15}\text{Al}_{0.05}\text{O}_2 \cdot x\text{Li}_2\text{MnO}_3 \cdot y\text{LiCoO}_2$

Novel cathode materials with improved performance should be obtained by building this ternary diagram between iso structural two-dimensional layered oxide cathode materials via  $\text{LiCoO}_2$ ,  $\text{Li}_2\text{MnO}_3(\text{Li}[\text{Li}_{1/3}\text{Mn}_{2/3}]\text{O}_2)$  and  $\text{LiNi}_{0.8}\text{Co}_{0.15}\text{Al}_{0.05}\text{O}_2$ .

## Chapter 5 Results and Discussion

### 5.1 System Overview

The ternary diagram with these three materials as end points is considered to be the system. The chosen end point materials are  $\text{LiCoO}_2$ ,  $\text{Li}_2\text{MnO}_3(\text{Li}[\text{Li}_{1/3}\text{Mn}_{2/3}]\text{O}_2)$  and  $\text{LiNi}_{0.8}\text{Co}_{0.15}\text{Al}_{0.05}\text{O}_2$ .  $\text{LiCoO}_2$  has a high capacity material but it suffers safety and cost issues. These issues are reduced using  $\text{LiNi}_{0.8}\text{Co}_{0.15}\text{Al}_{0.05}\text{O}_2$ , which is reported to have improved safety and cyclability. To further improve stability and safety electrochemically inert  $\text{Li}_2\text{MnO}_3$  is added as the third end point. It is anticipated that when combined these materials will provide properties that were not found in individual materials.



On the ternary diagram, 28 points are chosen for synthesis. These points are chosen to elucidate the capacity and cyclability trends of the entire system. The composition at each point is calculated by using the lever rule similar to the lever rule applied for binary diagrams. The lever rule states that “The relative amounts of two coexisting phases are inversely proportional to their distances from a point”. The first step in lever rule calculation is to draw a tie line through the composition. Next one measures the lengths of the tie line, and the distance from the composition to each end point. The relative amount of a material is proportional to the distance from the other material to the composition, divided by the length of the tie line. (Opposite length / total length).

**Table 2. Theoretical Compositions of the 28 points in the system (1-x-y)  $\text{LiNi}_{0.8}\text{Co}_{0.15}\text{Al}_{0.05}\text{O}_2 \cdot x\text{Li}_2\text{MnO}_3 \cdot y\text{LiCoO}_2$**

No	Composition	No	Composition
1	$\text{Li}_{1.0}\text{Ni}_{0.8}\text{Co}_{0.15}\text{Al}_{0.05}\text{Mn}_{0.0}$	15	$\text{Li}_{1.00}\text{Ni}_{0.267}\text{Co}_{0.717}\text{Al}_{0.017}\text{Mn}_{0.000}$
2	$\text{Li}_{1.167}\text{Ni}_{0.667}\text{Co}_{0.125}\text{Al}_{0.042}\text{Mn}_{0.167}$	16	$\text{Li}_{1.833}\text{Ni}_{0.133}\text{Co}_{0.025}\text{Al}_{0.008}\text{Mn}_{0.833}$
3	$\text{Li}_{1.0}\text{Ni}_{0.667}\text{Co}_{0.292}\text{Al}_{0.042}\text{Mn}_{0.0}$	17	$\text{Li}_{1.667}\text{Ni}_{0.133}\text{Co}_{0.192}\text{Al}_{0.008}\text{Mn}_{0.667}$
4	$\text{Li}_{1.333}\text{Ni}_{0.533}\text{Co}_{0.1}\text{Al}_{0.03}\text{Mn}_{0.33}$	18	$\text{Li}_{1.500}\text{Ni}_{0.133}\text{Co}_{0.358}\text{Al}_{0.008}\text{Mn}_{0.500}$
5	$\text{Li}_{1.167}\text{Ni}_{0.533}\text{Co}_{0.267}\text{Al}_{0.033}\text{Mn}_{0.167}$	19	$\text{Li}_{1.333}\text{Ni}_{0.333}\text{Co}_{0.525}\text{Al}_{0.008}\text{Mn}_{0.333}$
6	$\text{Li}_{1.00}\text{Ni}_{0.533}\text{Co}_{0.433}\text{Al}_{0.033}\text{Mn}_{0.0}$	20	$\text{Li}_{1.167}\text{Ni}_{0.133}\text{Co}_{0.692}\text{Al}_{0.008}\text{Mn}_{0.167}$
7	$\text{Li}_{1.5}\text{Ni}_{0.400}\text{Co}_{0.075}\text{Al}_{0.025}\text{Mn}_{0.5}$	21	$\text{Li}_{1.000}\text{Ni}_{0.133}\text{Co}_{0.858}\text{Al}_{0.008}\text{Mn}_{0.000}$

8	$\text{Li}_{1.333}\text{Ni}_{0.400}\text{Co}_{0.242}\text{Al}_{0.025}\text{Mn}_{0.333}$	22	$\text{Li}_{2.000}\text{Ni}_{0.000}\text{Co}_{0.000}\text{Al}_{0.000}\text{Mn}_{1.000}$
9	$\text{Li}_{1.167}\text{Ni}_{0.400}\text{Co}_{0.408}\text{Al}_{0.025}\text{Mn}_{0.167}$	23	$\text{Li}_{1.833}\text{Ni}_{0.000}\text{Co}_{0.167}\text{Al}_{0.000}\text{Mn}_{0.833}$
10	$\text{Li}_{1.000}\text{Ni}_{0.400}\text{Co}_{0.575}\text{Al}_{0.025}\text{Mn}_{0.000}$	24	$\text{Li}_{1.667}\text{Ni}_{0.000}\text{Co}_{0.333}\text{Al}_{0.000}\text{Mn}_{0.667}$
11	$\text{Li}_{1.667}\text{Ni}_{0.267}\text{Co}_{0.050}\text{Al}_{0.017}\text{Mn}_{0.667}$	25	$\text{Li}_{1.500}\text{Ni}_{0.000}\text{Co}_{0.500}\text{Al}_{0.000}\text{Mn}_{0.500}$
12	$\text{Li}_{1.500}\text{Ni}_{0.267}\text{Co}_{0.217}\text{Al}_{0.017}\text{Mn}_{0.500}$	26	$\text{Li}_{1.333}\text{Ni}_{0.000}\text{Co}_{0.667}\text{Al}_{0.000}\text{Mn}_{0.333}$
13	$\text{Li}_{1.333}\text{Ni}_{0.267}\text{Co}_{0.383}\text{Al}_{0.017}\text{Mn}_{0.333}$	27	$\text{Li}_{1.167}\text{Ni}_{0.000}\text{Co}_{0.833}\text{Al}_{0.000}\text{Mn}_{0.167}$
14	$\text{Li}_{1.167}\text{Ni}_{0.267}\text{Co}_{0.550}\text{Al}_{0.017}\text{Mn}_{0.167}$	28	$\text{Li}_{1.000}\text{Ni}_{0.000}\text{Co}_{1.000}\text{Al}_{0.000}\text{Mn}_{0.000}$

Nickel and Aluminum content decreases as we go down the triangle and samples 22, 24 have zero Ni and Al content. High Manganese content is found at sample 22 and the content decreases at the other end points of the triangle. Cobalt content is found in most of the regions in the triangle and it decreases near  $\text{Li}_2\text{MnO}_3$ . It is anticipated that capacity and cyclability of the samples were found to be directly related to the amount of Co, Mn, Al and Ni [25].

## 5.2 XRD

The crystal structure details and the phase purity were examined by Scintag X-ray diffraction using Cu-  $K_\alpha$  radiation. The diffraction patterns in comparison with International Centre for Diffraction Data showed that synthesized materials are single phase and can be indexed to lattice space R-3m with lattice constants. The lattice constants are indexed on sample #4. The layered structure of  $\text{LiCoO}_2$  can be explained as layers of Li and transition material Co (Co is present as  $\text{Co}^{3+}$ ) separated by oxygen. The shoulder peaks (003) and (101) are due to two crystal phases

existing in the samples [20]. Han et al [21] showed that calcination of  $\text{LiNi}_{0.8}\text{Co}_{0.15}\text{Al}_{0.05}\text{O}_2$  in flowing oxygen provides better structural stability for the material.

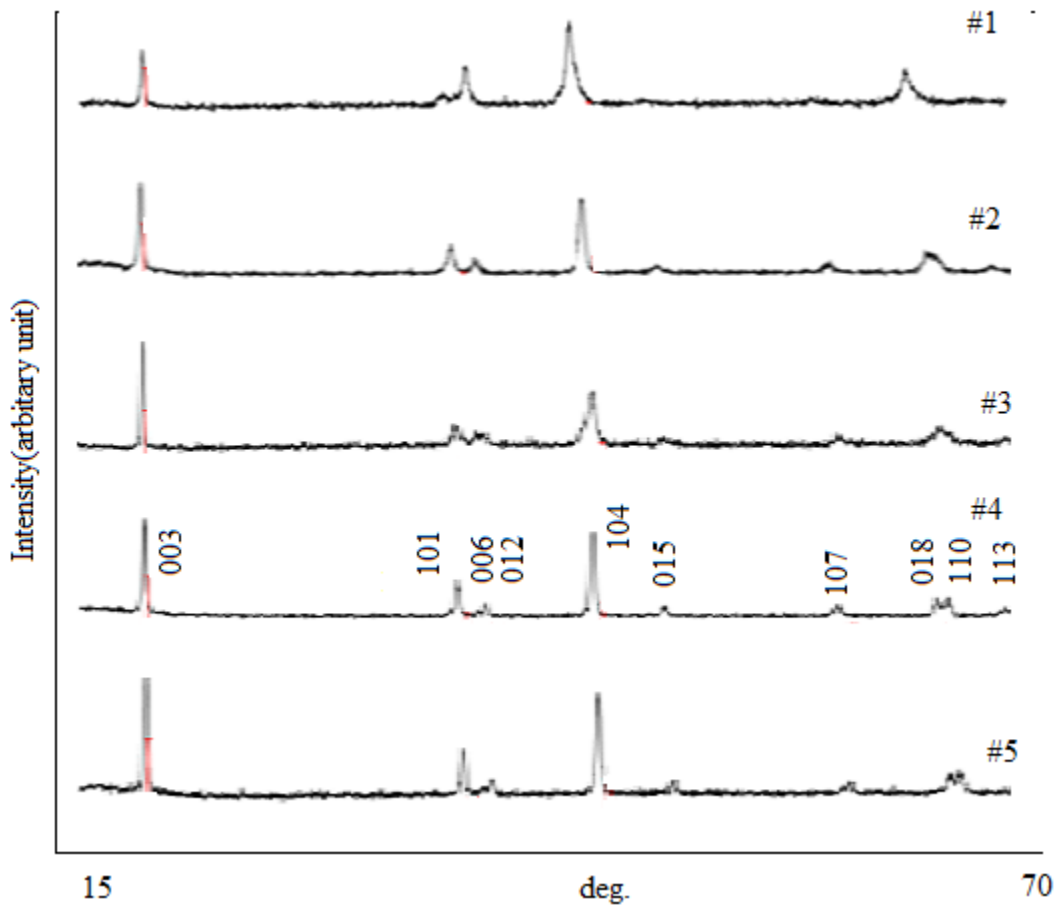


**Figure 22. XRD patterns of the system  $(1-x-y)\text{LiNi}_{0.8}\text{Co}_{0.15}\text{Al}_{0.05}\text{O}_2 \cdot x\text{Li}_2\text{MnO}_3 \cdot y\text{LiCoO}_2$  for samples 1 to 5**

Sample 1 ( $\text{LiNi}_{0.8}\text{Co}_{0.15}\text{Al}_{0.05}\text{O}_2$ ) had no peak at (107) which might be result of using the same synthesis conditions for all compositions. Perhaps the synthesis conditions were not adequate for this composition [26].

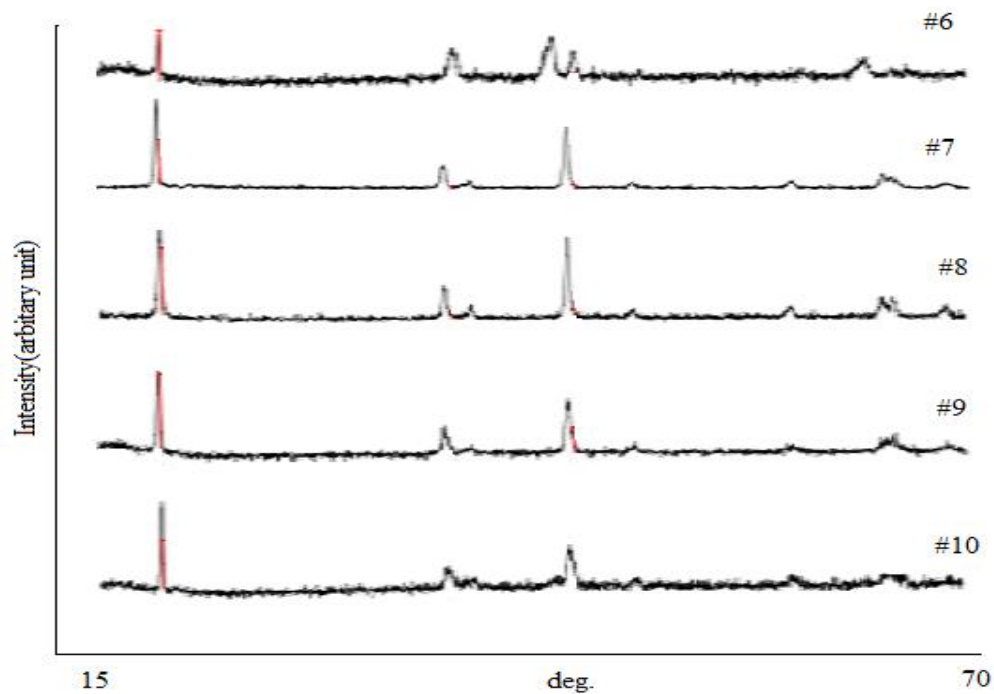


**Figure 23. XRD patterns of the system  $(1-x-y)$   $\text{LiNi}_{0.8}\text{Co}_{0.15}\text{Al}_{0.05}\text{O}_2 \cdot x\text{Li}_2\text{MnO}_3 \cdot y\text{LiCoO}_2$  for samples 6 to 10**

Sample #6 shows a split peak at (104) which might due to impurities during synthesis.

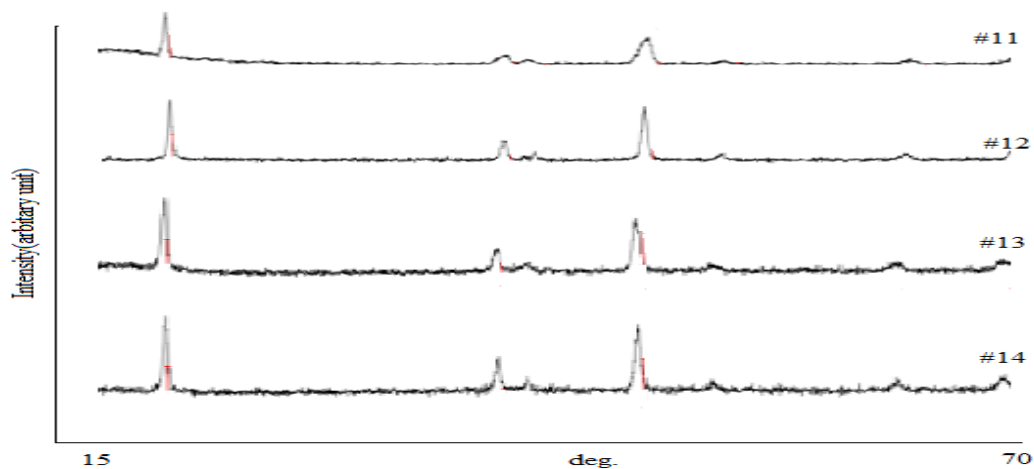


**Figure 24. XRD patterns of the system  $(1-x-y)$   $\text{LiNi}_{0.8}\text{Co}_{0.15}\text{Al}_{0.05}\text{O}_2 \cdot x\text{Li}_2\text{MnO}_3 \cdot y\text{LiCoO}_2$  for samples 11 to 14**

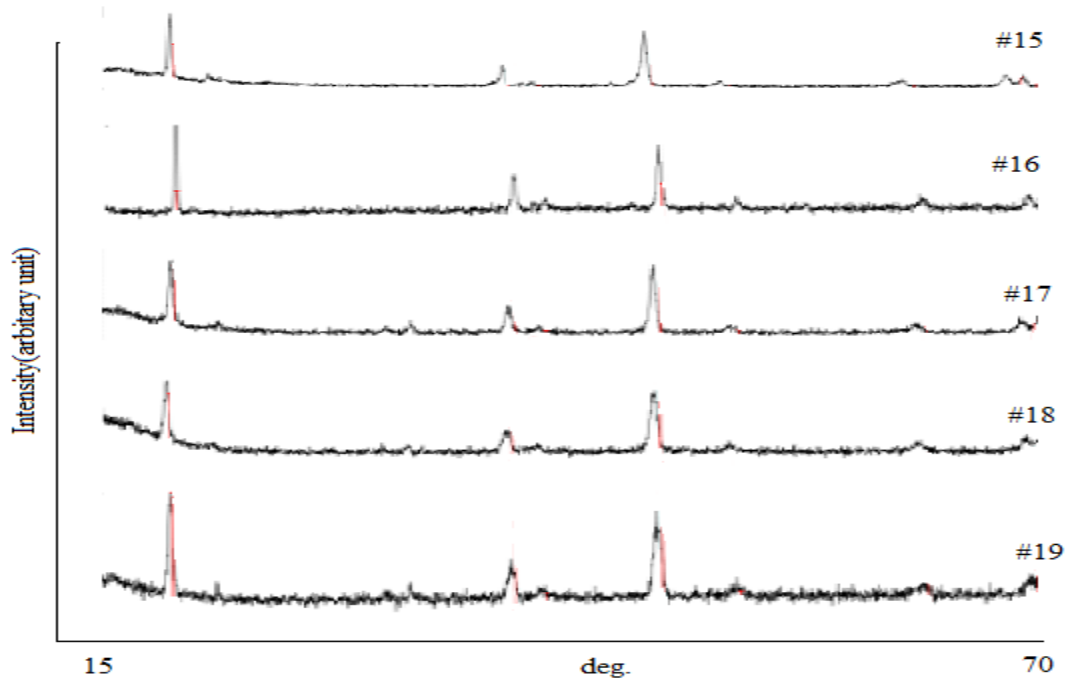


**Figure 25. XRD patterns of the system  $(1-x-y)$   $\text{LiNi}_{0.8}\text{Co}_{0.15}\text{Al}_{0.05}\text{O}_2 \cdot x\text{Li}_2\text{MnO}_3 \cdot y\text{LiCoO}_2$  for samples 15 to 19**

The unusual peaks in the samples 22 and 23 can be explained by superlattice ordering of  $\text{Mn}^{4+}$ , which induces superlattice reflection and reduces symmetry of  $\text{Li}_2\text{MnO}_3$  from R-3m to C-2m[29].

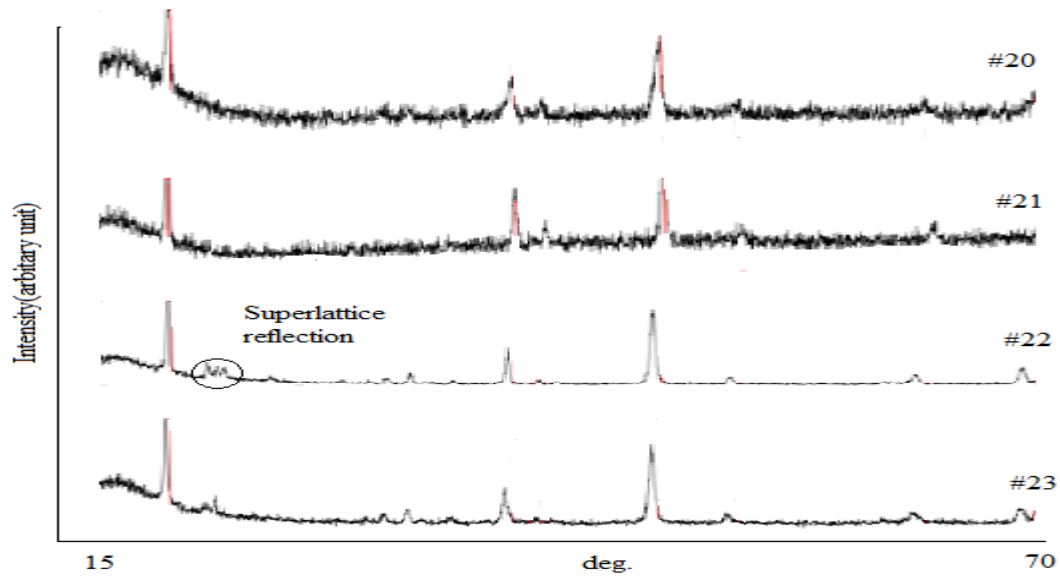


Figure 26. XRD patterns of the system  $(1-x-y) \text{LiNi}_{0.8}\text{Co}_{0.15}\text{Al}_{0.05}\text{O}_2 \cdot x\text{Li}_2\text{MnO}_3 \cdot y\text{LiCoO}_2$  for samples 20 to 23

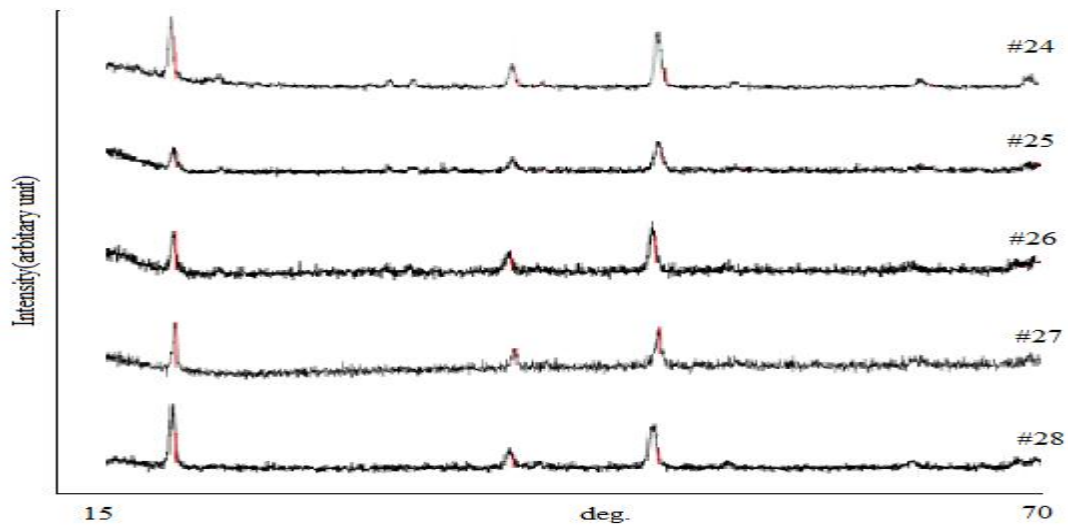
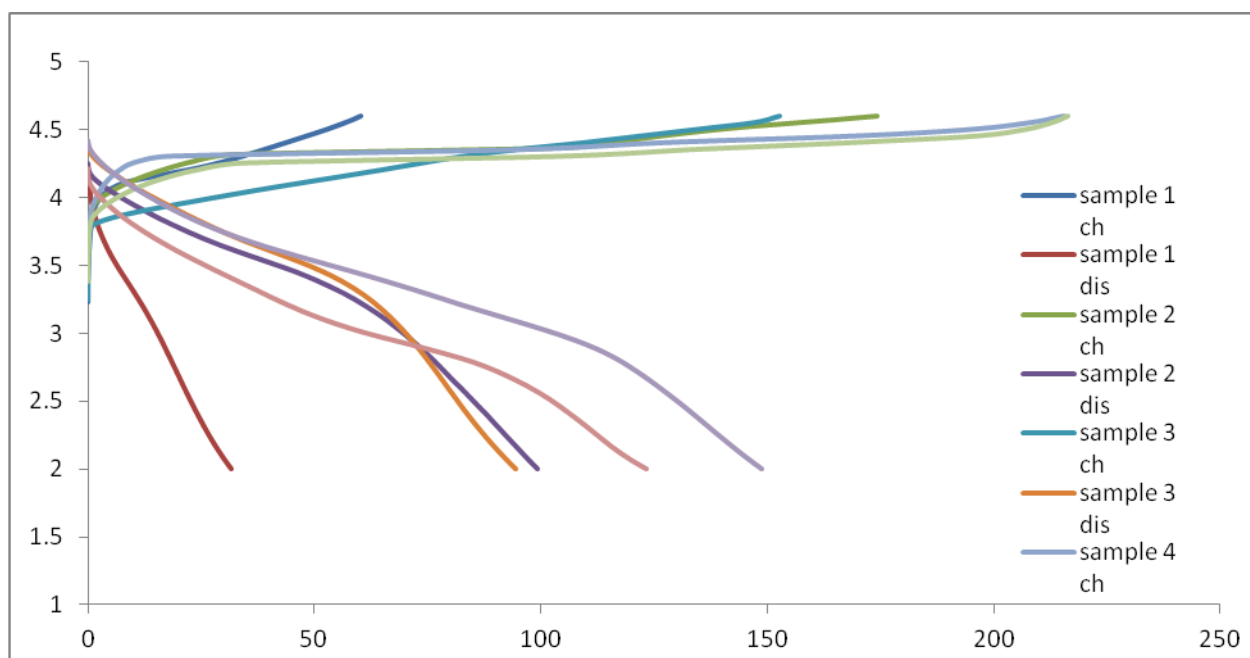


Figure 27. XRD patterns of the system  $(1-x-y) \text{LiNi}_{0.8}\text{Co}_{0.15}\text{Al}_{0.05}\text{O}_2 \cdot x\text{Li}_2\text{MnO}_3 \cdot y\text{LiCoO}_2$  for samples 24 to 28

Some samples have seen an aperture at the beginning of the scan, which is due to the reflection of the sample holder.

### 5.3 Electrochemical Testing

The electrochemical performances of cathodes were tested using Arbin BT2000 and MITS Pro Arbin software. The cycling was done between 2-4.6V with constant C-rate of C/15 at room temperature. All the samples were cycled for 10 cycles. Figures 27-31 show the charge and discharge curves plotted between Voltage (V) and capacity (mAh/g). All figures are plotted with the same scale for easier comparison between samples.



**Figure 28. Initial charge-discharge curves of samples 1 to 5**

Samples 1 to 5 (Figure 28) have shown lower capacity retention. The capacities were found to be in ascending order for sample one to five, which means that end member  $\text{LiNi}_{0.8}\text{Co}_{0.15}\text{Al}_{0.05}\text{O}_2$  had a significant deleterious effect on their capacities

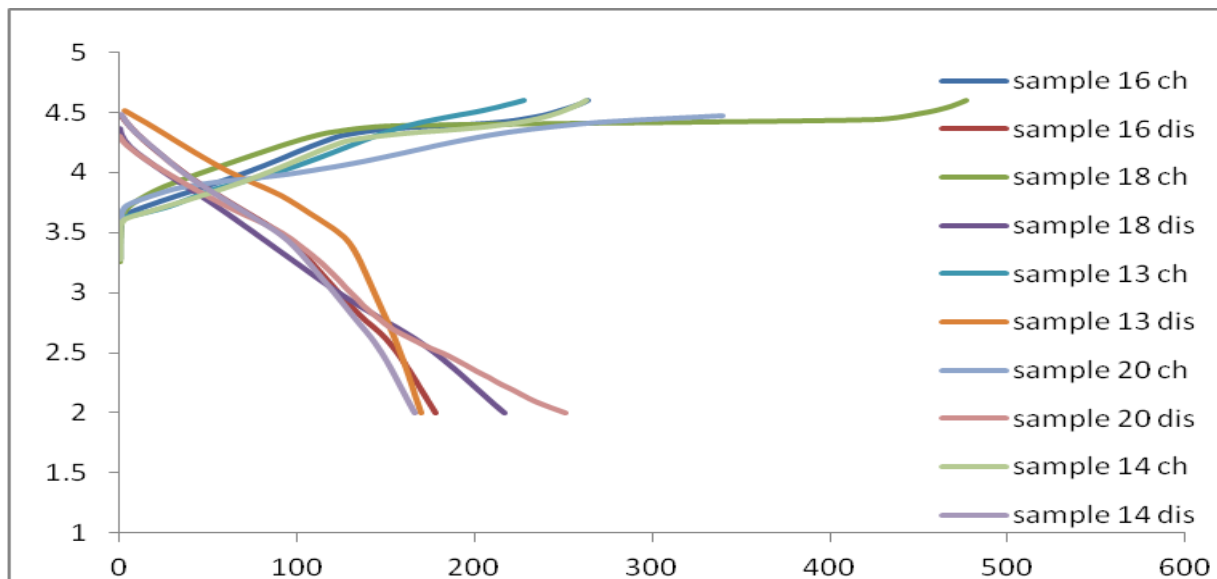


**Figure 29. Initial charge-discharge curves of samples 16,18,13,20 and 14**

Samples 16,18,13,20,14 ( Figure 29) have better capacity and cyclability properties than the rest of them. The samples closer to end member  $\text{Li}_2\text{MnO}_3$  have high cyclability as expected. Higher capacities can be related to more  $\text{Li}^+$  ions in the material which results in higher intercalation. Samples closer to  $\text{LiCoO}_2$  have capacity fading due to internal resistance accumulation [28].

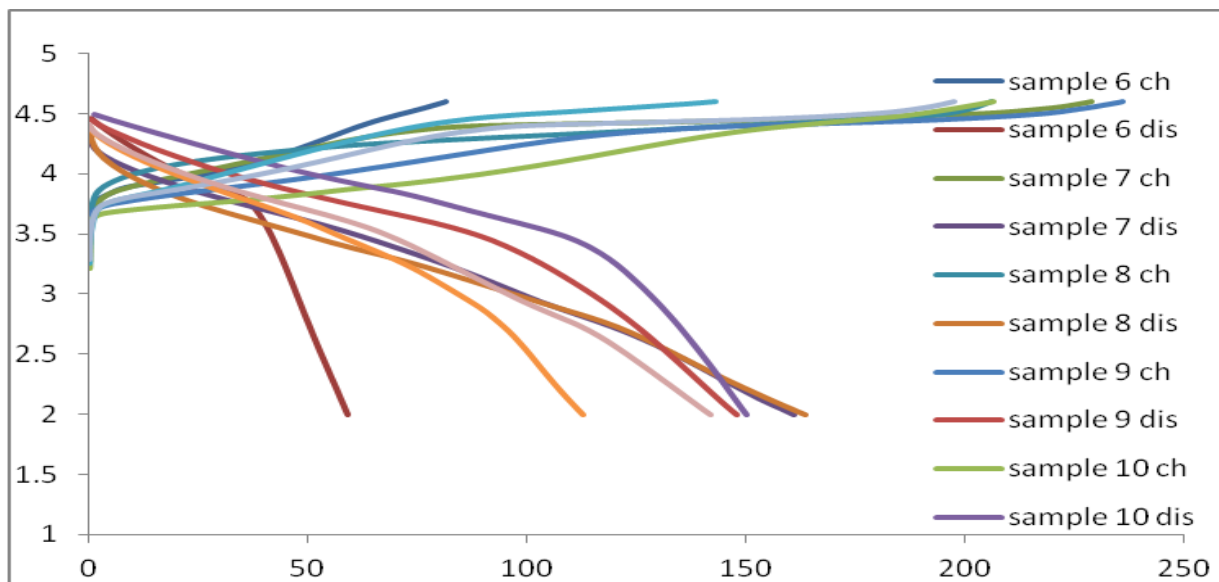


**Figure 30. Initial charge-discharge curves of samples 6 to 12**

Samples 6 to 12 (Figure 30) are placed near the centre of the ternary composition triangle. They have moderate amounts of capacity fading and fairly reasonable capacities.

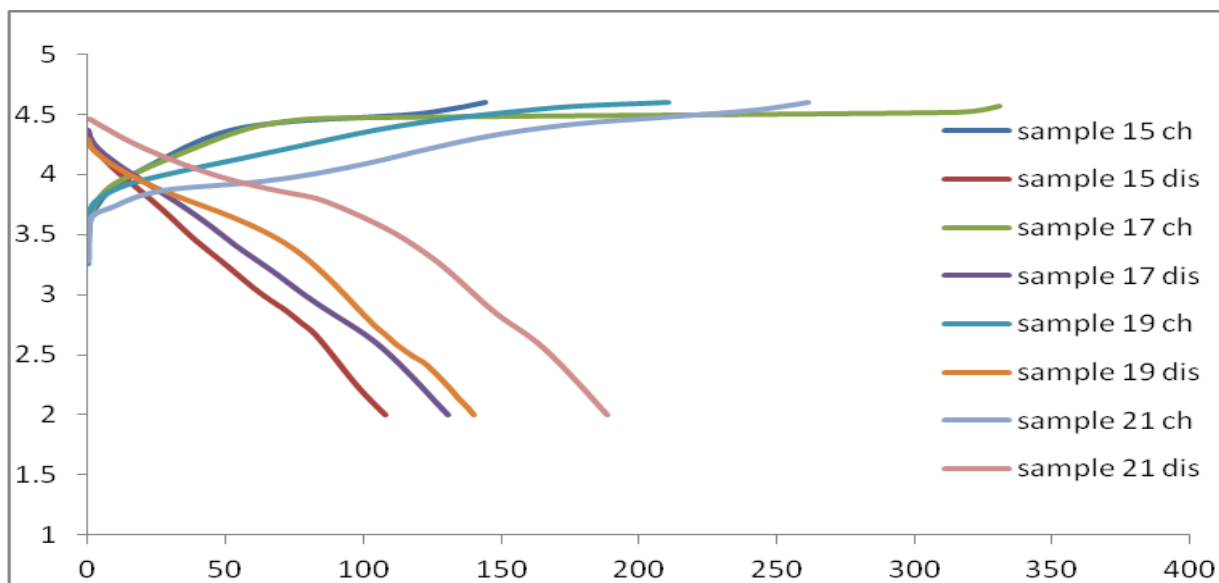


**Figure 31. Initial charge-discharge curves of samples 15,17,19 and 21**

Samples 15,17,19,21 (Figure 31) show good capacity retention but low capacity values.

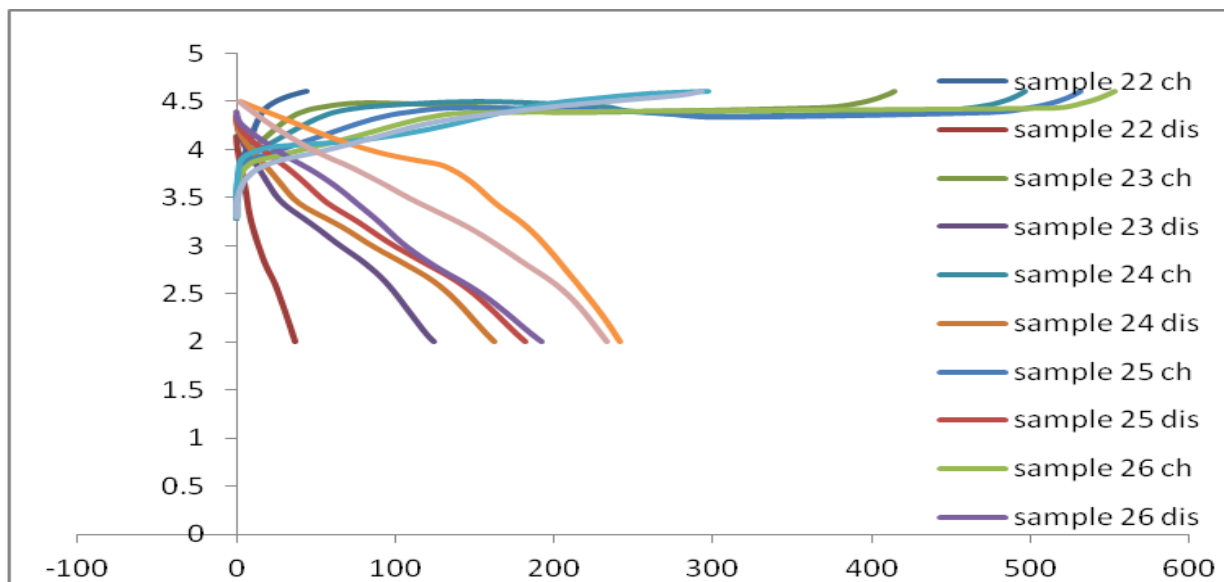


**Figure 32. Initial charge-discharge curves of samples 22 to 28**

The results show a wide range of capacities. The discharge curves are S-shaped. The capacities varied from 32 mAh/g to 250 mAh/g. The capacity and cyclability increase as we go from  $\text{LiNi}_{0.8}\text{Co}_{0.15}\text{Al}_{0.05}\text{O}_2$  towards the binary composition of  $\text{LiCoO}_2$  and  $\text{Li}_2\text{MnO}_3$

The curves show a long voltage drop below 3.5V resulting in good capacity performance. The kink in the curve at that voltage is due to lithium extraction from the material and oxygen loss in the form of  $\text{Li}_2\text{O}$ . Although sample 20 shows high capacity of 250.4 mAh/g, it suffers from low cyclability. The sample 18 shows a good capacity material of 216.3 mAh/g with an ability to retain the capacity for a multiple cycles. Sample 22 ( $\text{Li}_2\text{MnO}_3$ ) suffers from low capacity as  $\text{Mn}^{4+}$  is inert and it must rely on  $\text{O}_2$  loss to show reversible capacity.

**Table 3. Theoretical composition, capacity and cyclability of the system (1-x-y)  $\text{LiNi}_{0.8}\text{Co}_{0.15}\text{Al}_{0.05}\text{O}_2 \cdot x\text{Li}_2\text{MnO}_3$  summary.**

No	Composition	Capacity (mAh/g)	Cyclability (%)
1	$\text{Li}_{1.0}\text{Ni}_{0.8}\text{Co}_{0.15}\text{Al}_{0.05}\text{Mn}_{0.0}$	31.8	49.2
2	$\text{Li}_{1.167}\text{Ni}_{0.667}\text{Co}_{0.125}\text{Al}_{0.042}\text{Mn}_{0.167}$	99.19	41.0
3	$\text{Li}_{1.0}\text{Ni}_{0.667}\text{Co}_{0.292}\text{Al}_{0.042}\text{Mn}_{0.0}$	94.43	40
4	$\text{Li}_{1.333}\text{Ni}_{0.533}\text{Co}_{0.1}\text{Al}_{0.03}\text{Mn}_{0.33}$	123.43	48.9
5	$\text{Li}_{1.167}\text{Ni}_{0.533}\text{Co}_{0.267}\text{Al}_{0.033}\text{Mn}_{0.167}$	148.76	65
6	$\text{Li}_{1.00}\text{Ni}_{0.533}\text{Co}_{0.433}\text{Al}_{0.033}\text{Mn}_{0.0}$	59.16	83.2
7	$\text{Li}_{1.5}\text{Ni}_{0.400}\text{Co}_{0.075}\text{Al}_{0.025}\text{Mn}_{0.5}$	160.97	86.05
8	$\text{Li}_{1.333}\text{Ni}_{0.400}\text{Co}_{0.242}\text{Al}_{0.025}\text{Mn}_{0.333}$	163.57	63.19
9	$\text{Li}_{1.167}\text{Ni}_{0.400}\text{Co}_{0.408}\text{Al}_{0.025}\text{Mn}_{0.167}$	147.79	83.8
10	$\text{Li}_{1.000}\text{Ni}_{0.400}\text{Co}_{0.575}\text{Al}_{0.025}\text{Mn}_{0.000}$	150.11	82.8

11	$\text{Li}_{1.667}\text{Ni}_{0.267}\text{Co}_{0.050}\text{Al}_{0.017}\text{Mn}_{0.667}$	112.58	100
12	$\text{Li}_{1.500}\text{Ni}_{0.267}\text{Co}_{0.217}\text{Al}_{0.017}\text{Mn}_{0.500}$	141.69	100
13	$\text{Li}_{1.333}\text{Ni}_{0.267}\text{Co}_{0.383}\text{Al}_{0.017}\text{Mn}_{0.333}$	169.9	80.6
14	$\text{Li}_{1.167}\text{Ni}_{0.267}\text{Co}_{0.550}\text{Al}_{0.017}\text{Mn}_{0.167}$	166.16	85
15	$\text{Li}_{1.00}\text{Ni}_{0.267}\text{Co}_{0.717}\text{Al}_{0.017}\text{Mn}_{0.000}$	108.14	100
16	$\text{Li}_{1.833}\text{Ni}_{0.133}\text{Co}_{0.025}\text{Al}_{0.008}\text{Mn}_{0.833}$	178.13	87.8
17	$\text{Li}_{1.667}\text{Ni}_{0.133}\text{Co}_{0.192}\text{Al}_{0.008}\text{Mn}_{0.667}$	130.62	100
18	$\text{Li}_{1.500}\text{Ni}_{0.133}\text{Co}_{0.358}\text{Al}_{0.008}\text{Mn}_{0.500}$	216.38	100
19	$\text{Li}_{1.333}\text{Ni}_{0.333}\text{Co}_{0.525}\text{Al}_{0.008}\text{Mn}_{0.333}$	140.05	100
20	$\text{Li}_{1.167}\text{Ni}_{0.133}\text{Co}_{0.692}\text{Al}_{0.008}\text{Mn}_{0.167}$	250.8	76.9
21	$\text{Li}_{1.000}\text{Ni}_{0.133}\text{Co}_{0.858}\text{Al}_{0.008}\text{Mn}_{0.000}$	188.4	94.2
22	$\text{Li}_{2.000}\text{Ni}_{0.000}\text{Co}_{0.000}\text{Al}_{0.000}\text{Mn}_{1.000}$	37.3	100

23	$\text{Li}_{1.833}\text{Ni}_{0.000}\text{Co}_{0.167}\text{Al}_{0.000}\text{Mn}_{0.833}$	123.98	100
24	$\text{Li}_{1.667}\text{Ni}_{0.000}\text{Co}_{0.333}\text{Al}_{0.000}\text{Mn}_{0.667}$	162.54	100
25	$\text{Li}_{1.500}\text{Ni}_{0.000}\text{Co}_{0.500}\text{Al}_{0.000}\text{Mn}_{0.500}$	191.8	100
26	$\text{Li}_{1.333}\text{Ni}_{0.000}\text{Co}_{0.667}\text{Al}_{0.000}\text{Mn}_{0.333}$	181.62	100
27	$\text{Li}_{1.167}\text{Ni}_{0.000}\text{Co}_{0.833}\text{Al}_{0.000}\text{Mn}_{0.167}$	240.95	87.9
28	$\text{Li}_{1.000}\text{Ni}_{0.000}\text{Co}_{1.000}\text{Al}_{0.000}\text{Mn}_{0.000}$	233.47	98.1

#### 5.4 Statistical Analysis

Statistical analysis was used to find the area of best response from the collected data, so that the most promising of the 28 compositions could be studied further. The software used was SAS/STAT 9.2 with the ADX procedure to fit a general linear model with three linear terms and three two-way interactions.

Tests with capacity and cyclability as criteria were run. For the first test, Y1 is capacity and X1,X2,X3 are  $\text{Li}_2\text{MnO}_3$ ,  $\text{Li}_2\text{CoO}_2$ ,  $\text{LiNi}_{0.8}\text{Co}_{0.15}\text{Al}_{0.05}\text{O}_2$  respectively. The table 3 shows the significance of the effects (end members in the ternary composition and their interactions)

**Table 4. Significance of end members and their interactions with capacity as criteria**

Effect	Estimate	Std Error	t Ratio	P Value
X1	63.885	23.061	2.7702	0.0112
X2	229.74	23.061	9.962	<.0001
X3	42.741	23.065	1.8531	0.0773
X1*X2	173.25	94.816	1.8272	0.0813
X1*X3	404.81	94.816	4.2695	0.0003
X2*X3	-56.504	94.819	-0.59591	0.5573

The rows highlighted in yellow indicate that the effect is significant. The interaction X1\*X3 is more significant than the other two interactions and all the end members are significant.

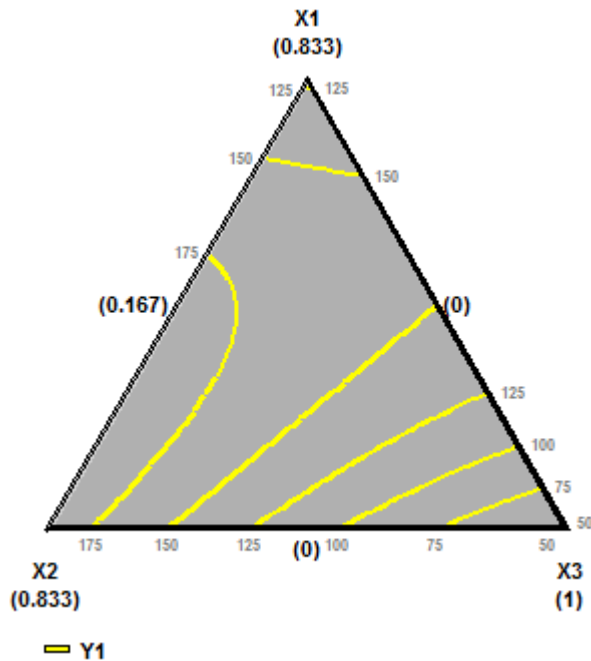


**Figure 33. Statistical analysis of the system with capacity as criteria**

The analysis shows capacity increase towards the interaction  $\text{Li}_2\text{MnO}_3$  and  $\text{LiNi}_{0.8}\text{Co}_{0.15}\text{Al}_{0.05}\text{O}_2$ . The yellow curves represent the capacity trends and capacity values are indicated on the boundaries. The capacity values in the range of 175 mAh/g.

For the second test, Y2 is cyclability and X1,X2,X3 are  $\text{Li}_2\text{MnO}_3$ ,  $\text{Li}_2\text{CoO}_2$ ,  $\text{LiNi}_{0.8}\text{Co}_{0.15}\text{Al}_{0.05}\text{O}_2$  respectively.

**Table 5. Significance of end members and their interactions with cyclability as criteria**

Effect	Estimate	Std Error	t Ratio	P Value
X1	104.89	7.5159	13.956	<.0001
X2	93.567	7.516	12.449	<.0001
X3	34.144	7.5172	4.5421	0.0002
X1*X2	-5.8206	30.902	-0.18836	0.8523
X1*X3	22.817	30.902	0.73839	0.4681
X2*X3	76.992	30.903	2.4914	0.0208

The following table 4 shows the significance of the effects (end members in the ternary diagram)

The rows highlighted in yellow indicate that the effect is significant. The interaction X2\*X3 is more significant than the other two interactions and all the end members are significant.

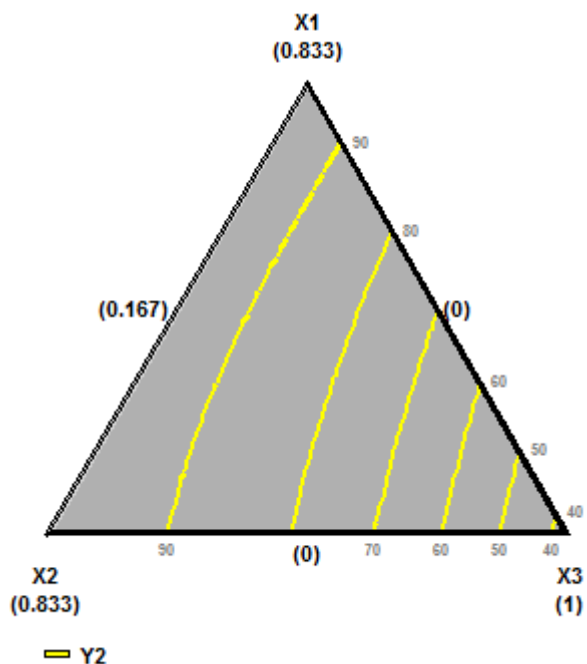


**Figure 34. Statistical analysis of the system with cyclability as criteria**

The analysis shows cyclability increase towards the interaction  $\text{Li}_2\text{MnO}_3$  and  $\text{LiNi}_{0.8}\text{Co}_{0.15}\text{Al}_{0.05}\text{O}_2$

Both models showed some general trends and also a more defined area of maximum capacity and cyclability. It projected a “sweet spot” near sample 18 with good capacity and cyclability numbers.

### 5.5 ICP-AES

Samples 1, 15, 18 and 20 were tested for their compositions using a Perkin Elmer Optima 7300 DV with a Cetac ASX-520 auto sampler

**Table 6: Comparison of measured and theoretical compositions using ICP-AES**

Sample No	Measured composition using ICP-AES	Theoretical composition
1	Li <sub>1.034</sub> Ni <sub>0.709</sub> Co <sub>0.19</sub> Al <sub>0.06</sub> Mn <sub>0.014</sub>	Li <sub>1.0</sub> Ni <sub>0.8</sub> Co <sub>0.15</sub> Al <sub>0.05</sub> Mn <sub>0.0</sub>
15	Li <sub>1.002</sub> Ni <sub>0.268</sub> Co <sub>0.708</sub> Al <sub>0.017</sub> Mn <sub>0.0035</sub>	Li <sub>1.0</sub> Ni <sub>0.267</sub> Co <sub>0.717</sub> Al <sub>0.017</sub> Mn <sub>0.0</sub>
18	Li <sub>1.384</sub> Ni <sub>0.0769</sub> Co <sub>0.244</sub> Al <sub>0.004</sub> Mn <sub>0.289</sub>	Li <sub>1.5</sub> Ni <sub>0.133</sub> Co <sub>0.358</sub> Al <sub>0.008</sub> Mn <sub>0.5</sub>
20	Li <sub>1.299</sub> Ni <sub>0.15</sub> Co <sub>0.52</sub> Al <sub>0.00348</sub> Mn <sub>0.126</sub>	Li <sub>1.167</sub> Ni <sub>0.133</sub> Co <sub>0.692</sub> Al <sub>0.008</sub> Mn <sub>0.167</sub>

The measured compositions and the theoretical compositions are in relatively good agreement for most of the samples.

### 5.6 Repeats

Based on the projections of statistical analysis, samples 16,18 and 20 were selected for repeats. Synthesis conditions of the original set of samples were followed for these repeat samples. However, sample #1 was also synthesized again under inert conditions (calcination was under inert atmosphere) in reference to [26].

The XRD results show that the repeats achieved the same structure as the original samples. The diffraction patterns in comparison with International Centre for Diffraction Data showed that synthesized materials are single phase and can be indexed to lattice space R-3m with lattice constants.

The repeats were made into T-Cells and subjected to electrochemical testing using the original conditions (the cycling was done between 2-4.6V with constant C-rate of C/15 at room temperature).

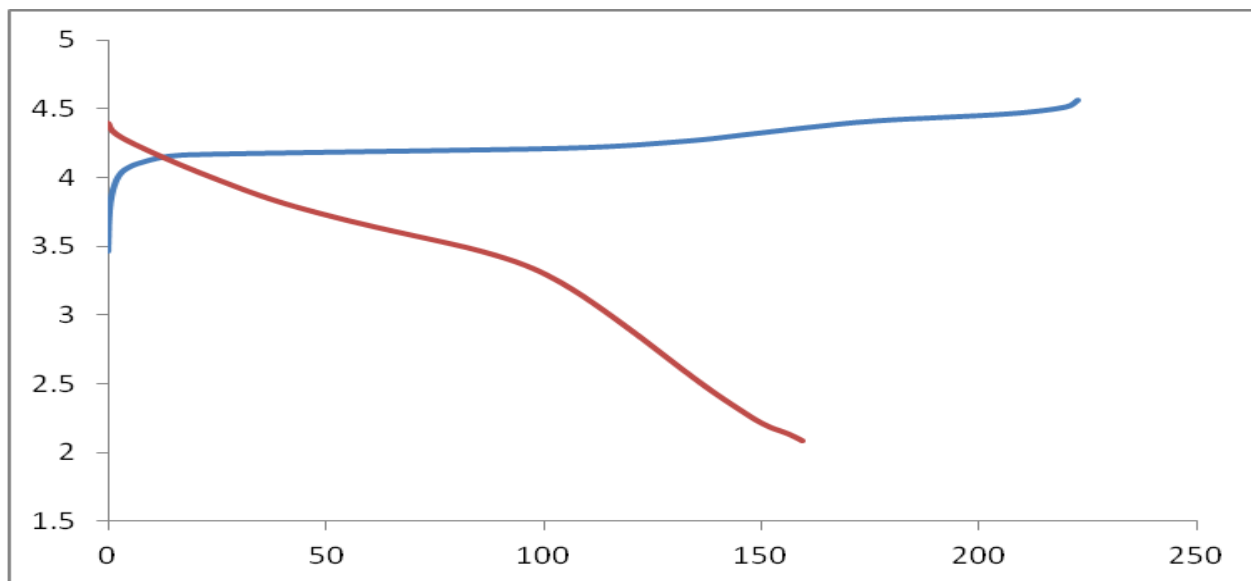


**Figure 35. Initial charge-discharge curves of repeat sample#1**

The repeat sample 1 shows better charge and discharge capacities (discharge capacity of 159 mAh/g) than the original sample. This improvement in the capacities is attributed to the synthesis conditions (repeat sample was cooked in inert conditions).

The repeat sample 18 showed lower irreversible capacity loss than the original, the discharge capacity of 200 mAh/g was close to the original. The recyclability matches the original.

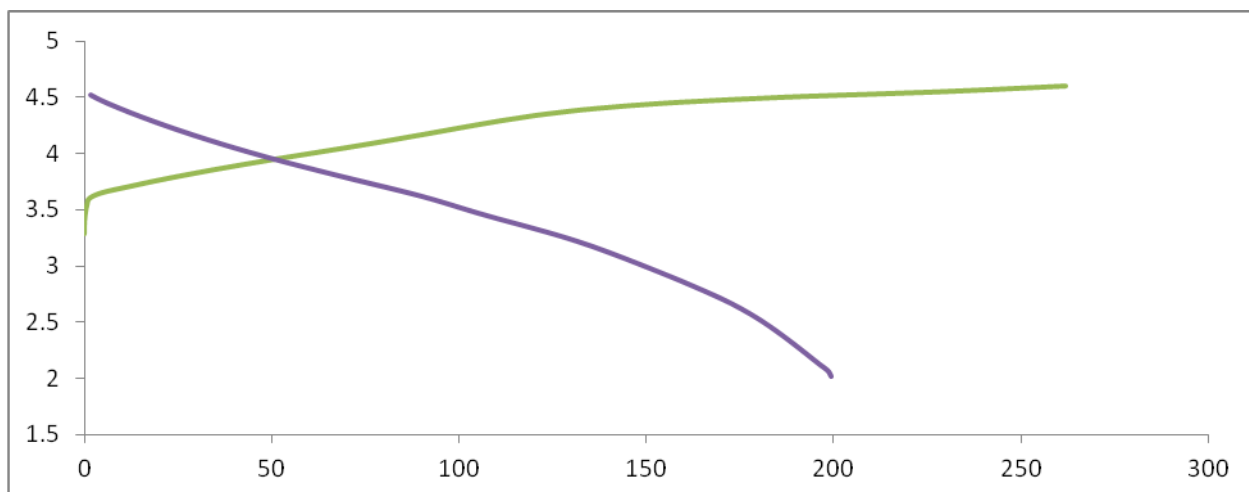


**Figure 36. Initial charge-discharge curves of repeat sample#18**

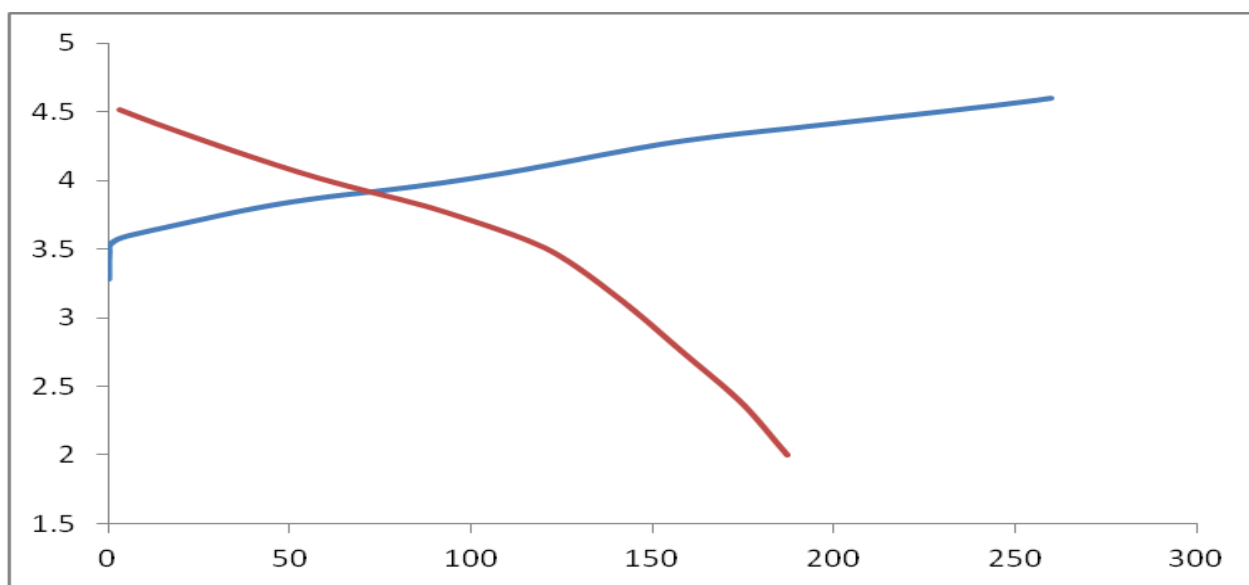


**Figure 37. Initial charge-discharge curves of repeat sample#20**

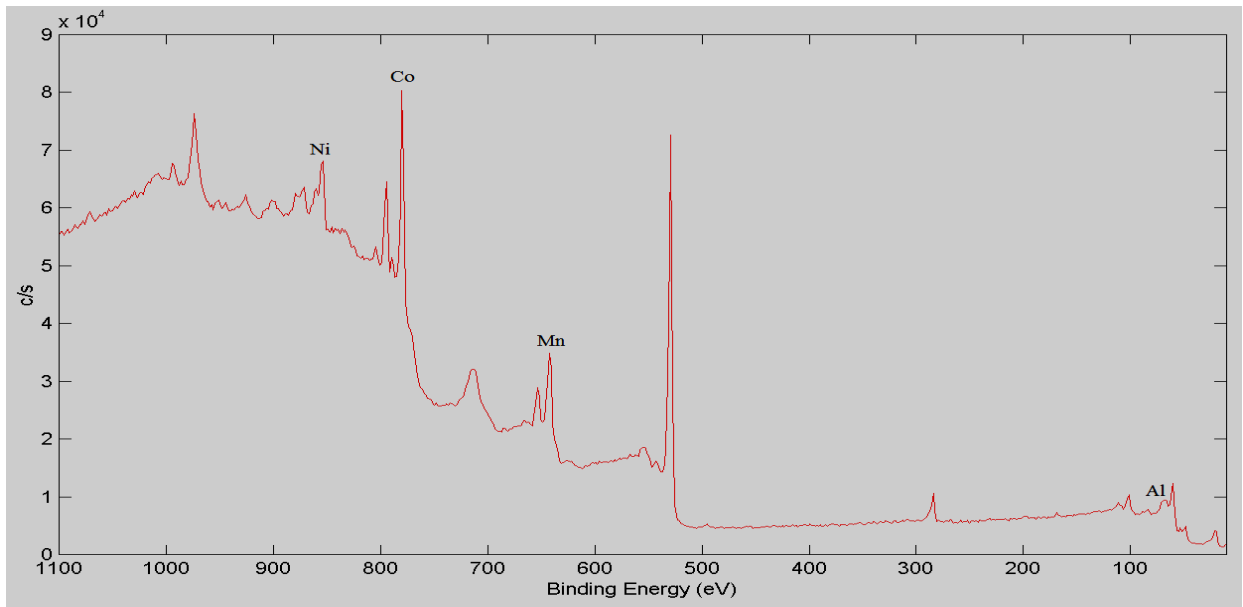
The repeat sample#20 showed a discharge capacity of 200 mAh/g and lower irreversible capacity loss. The cyclability was 83%. The table 5 shows the comparison of discharge capacities between the repeats and the original samples.

**Table 7. The comparison of discharge capacities between the repeats and the original samples.**

Sample No	Discharge capacity of original sample in mAh/g	Discharge capacity of repeat sample in mAh/g
1	31.8	159.82
18	216.38	200
20	250.8	188

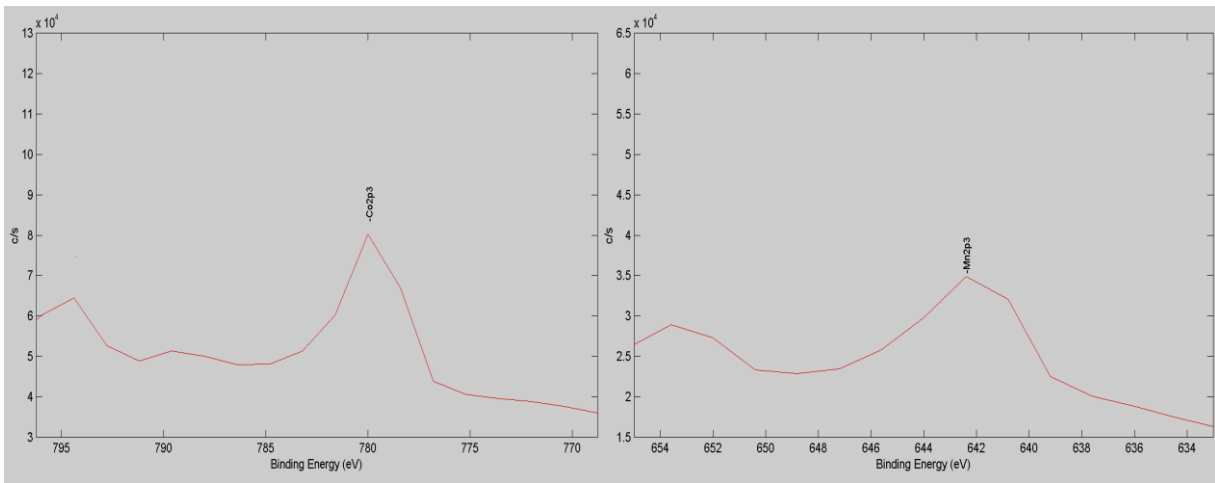
### 5.7 XPS

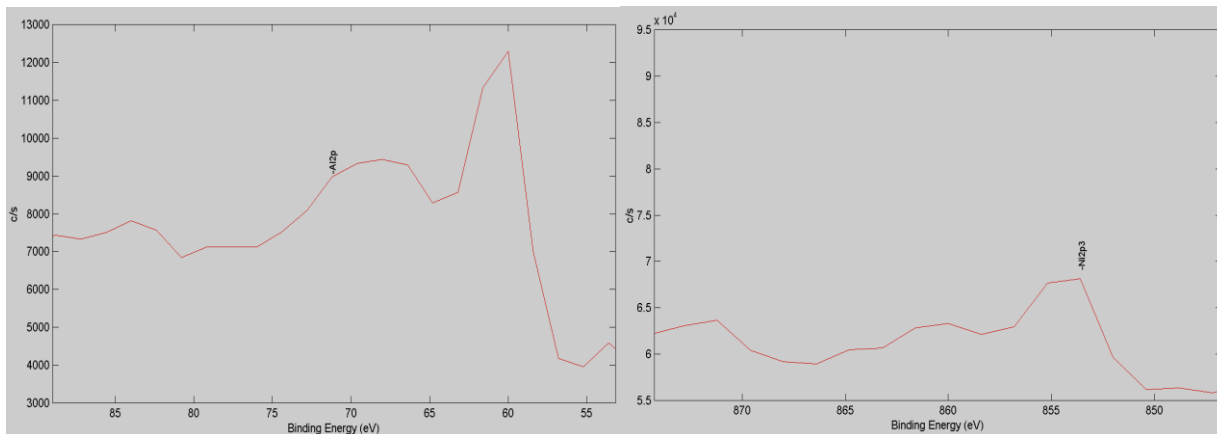
XPS measurement was performed on samples 16, 18 and 20 (before cycling) at room temperature to determine the valence state of the transitional metals in the system such as Ni, Mn, Co and post transition metal like Al by obtaining a full-scan spectrum which shows valence states of the elements.



**Figure 38. XPS spectra of sample#20**

Figure 36 shows the XPS scan of sample 20, main peaks of Al,Mn,Co and Al are marked on the spectra.

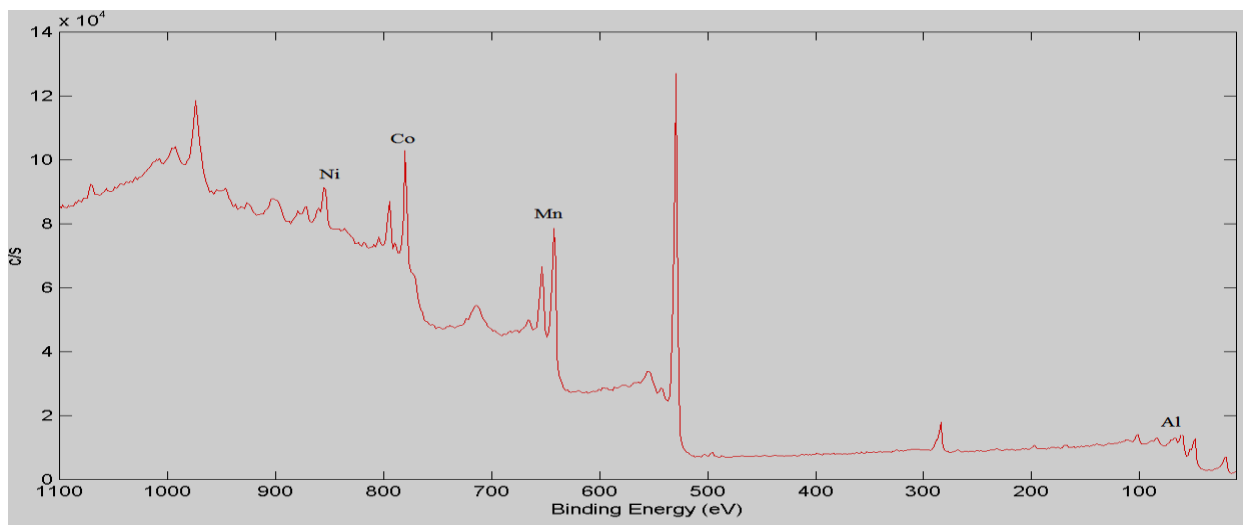




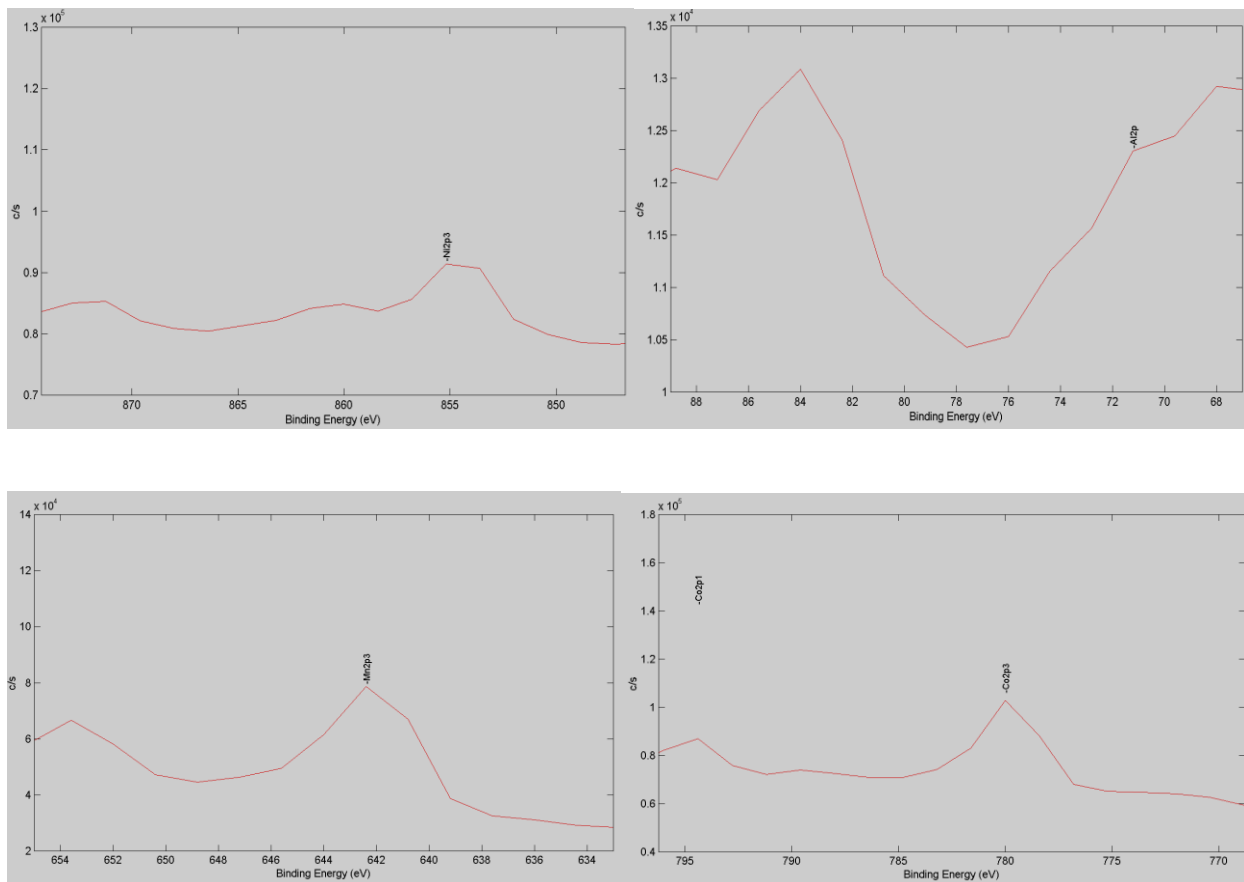
**Figure 39. Main peaks of Co,Mn,Al and Ni elements respectively for sample #20**

Figure 37 shows Co $2p_{3/2}$  main peak with a binding energy of 780.03eV which matches with binding energy of CoOOH that has cobalt in Co $^{+3}$  state. The main peak Mn $2p_{3/2}$  is with a binding energy of 642.6eV matches MnO $_2$  with Mn $^{+4}$  state. Al is found with a weak signal of binding energy 71.19eV of Al $^{+4}$  state because of its low amount. Ni $2p_{3/2}$  main peak had a binding energy of 854.4eV matches NiO of Ni $^{+2}$  oxidation state.

Figure 40 shows the full scan spectra of sample 18



**Figure 40. XPS spectra of sample#18**



**Figure 41. Main peaks of Co,Mn,Al and Ni elements for sample #18**

The main peaks were matched to their binding energies and the valence states were found to be  $\text{Co}^{+3}$ ,  $\text{Mn}^{+4}$ ,  $\text{Al}^{+4}$  and  $\text{Ni}^{+2}$ .

### 5.8 Discussion of Best Compositions

This section provides in depth discussion of samples 18 and 20. These two samples provided better capacity and cyclability properties than the remaining samples in the entire ternary composition.

### Sample 18

$\text{Li}_{1.5}\text{Ni}_{0.133}\text{Co}_{0.358}\text{Al}_{0.008}\text{Mn}_{0.5}$  is the theoretical composition of sample#18. The XRD results of the sample discussed in section 5.2 show single phase, figure 39 shows the electrochemical testing data with charge capacity of 261.91 mAh/g, discharge capacity of 200 mAh/g and a capacity retention of 96%.

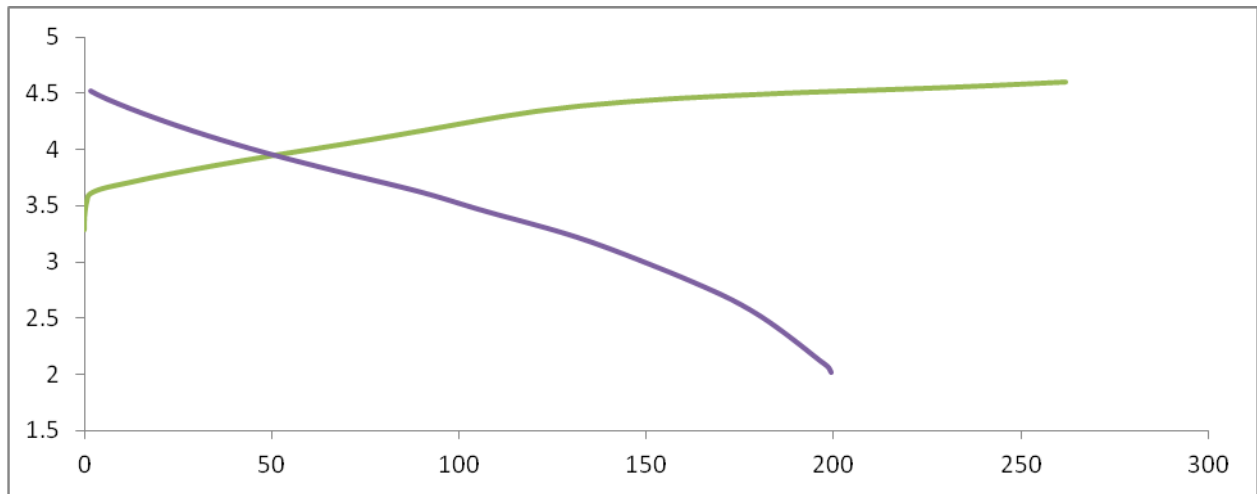


**Figure 42. Initial charge-discharge curves**

The green curve represents the charge curve of the sample. The difference between charge capacity and discharge capacity is called irreversible capacity loss. The irreversible charge plateau after 4.45V is because of  $\text{Li}_2\text{MnO}_3$  content in the sample which is due to removal  $\text{Li}_2\text{O}$  from the solid solution [20]. The blue curve represents the discharge curve, discharge capacity gradually increases after 4V due to  $\text{Li}^+$  re-insertion into the structure and from 4V to 2.8V Al content increases the performance and rate capability of the material [26]. The electrochemical performance showed the involvement of  $\text{Ni}^{4+}/\text{Ni}^{2+}$ ,  $\text{Co}^{4+}/\text{Co}^{3+}$  (oxidation) and  $\text{Mn}^{4+}, \text{Al}^{4+}$  remain stable [25]. The performance was also related to high Li content and optimum contents of Mn, Ni, Co and Al.

### Sample 20

$\text{Li}_{1.167}\text{Ni}_{0.133}\text{Co}_{0.692}\text{Al}_{0.008}\text{Mn}_{0.167}$  is the theoretical composition of sample#20. Electrochemical testing data show that charge capacity was 250.76mAh/g, discharge capacity was 187.31 mAh/g(repeat sample) and a capacity retention of 83%.

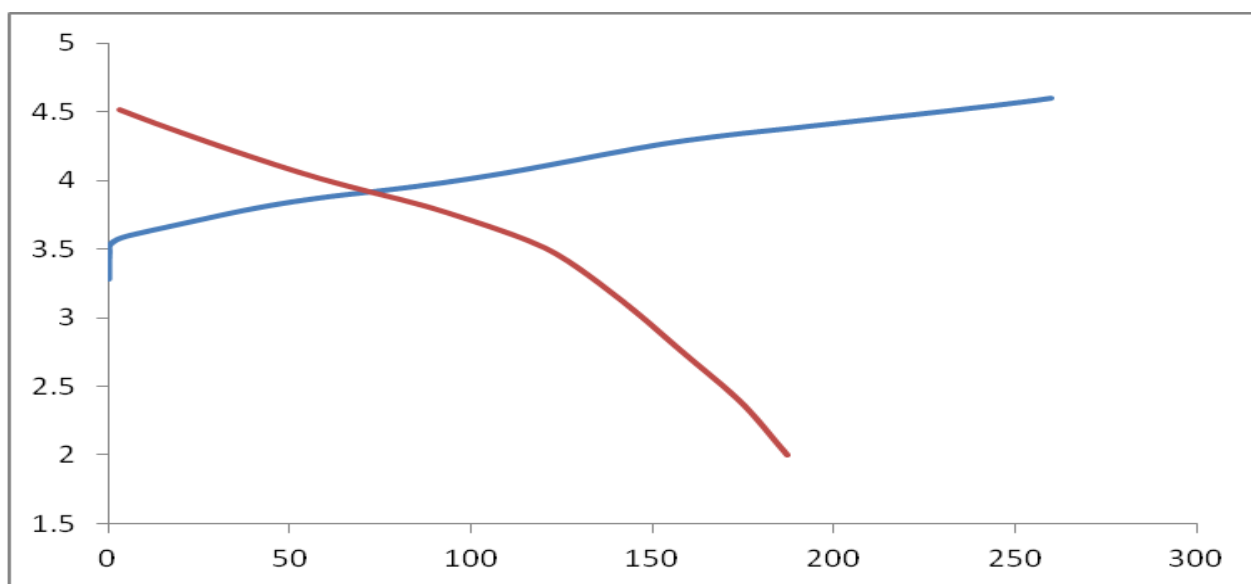


**Figure 43. Initial charge-discharge curves**

The original sample showed higher capacities than the repeat samples which might be due to discrepancies in synthesis. The irreversible charge plateau is found to be lower than sample 18, which might be because of low Mn content. Better performance in capacity is related to cobalt content. Increase in Co content influences not only adsorption of  $\text{O}_2$  but also oxidation states of Mn, Ni and Al[27].

Comparing the samples 18 and 20, sample #18 has better capacities and cyclability. Moreover, Cobalt content in sample #18 is low which makes the material both less toxic and less expensive

than the other sample. It can be concluded that sample#18 has the potential to become a commercial cathode material but it needs further analysis before commercialization.

## Chapter 6 Conclusions and Future work

The system  $(1-x-y) \text{LiNi}_{0.8}\text{Co}_{0.15}\text{Al}_{0.05}\text{O}_2 \cdot x\text{Li}_2\text{MnO}_3 \cdot y\text{LiCoO}_2$  is synthesized using a simple sol-gel synthesis. The materials  $\text{LiNi}_{0.8}\text{Co}_{0.15}\text{Al}_{0.05}\text{O}_2$ ,  $\text{Li}_2\text{MnO}_3$  and  $\text{LiCoO}_2$  were used as end points in a ternary composition diagram. Twenty eight cathode compositions spanning the entire ternary composition diagram were synthesized under the same conditions and characterized using X-ray diffraction (XRD), XPS, ICP-AES and an Arbin BT2000 battery testing system.

The repeats for the samples were made to check the consistency of the synthesis process. XRD data showed that all materials are single phase and can be indexed to lattice space R-3m with lattice constants. XPS data showed the oxidation states of the elements Ni, Co, Mn and Al. The accuracy of the measured composition was tested using ICP-AES. Statistical analysis was done using SAS/STAT 9.2 with the ADX procedure to fit a general linear model with three linear terms and three two way interactions to map capacities and cyclabilities. This analysis was used to choose the compositions with best capacities and cyclability. Inductively couple plasma (ICP) analysis was carried out on the chosen samples to find the error between calculated composition and the theoretical composition.

The electrochemical testing data results reveal that sample 18 and sample 20 have better capacity and cyclability properties than the other samples in the entire composition. Because of better capacity retention, cost and toxicity sample #18 with theoretical composition  $\text{Li}_{1.5}\text{Ni}_{0.133}\text{Co}_{0.358}\text{Al}_{0.008}\text{Mn}_{0.5}$  was chosen as the best sample. Sample 18 has a specific discharge capacity of 200mAh/g which is higher than the commercial  $\text{LiCoO}_2$  discharge capacity. The capacity retention of 96% is also higher than the commercial cathode retention.

Limitations of the present work include assuming the particle size to be 45  $\mu\text{m}$  without testing it; working on compositions across the entire ternary diagram, when a focus on concentrations near sample 18 and sample 20 would have been more efficient and might have yielded even better performance, lack of tests like impedance spectroscopy to see resistance build up on cathode surfaces.

As a future work, further analysis should be done on sample#18 before exploring the commercialization of the material. Differential scanning calorimetry can be used to explore the safety of the material under multiple cycles.

The particle size of the materials in the system was assumed to be 45 $\mu\text{m}$ . Particle size has been found to have a direct effect on the performance of the material [30] which can be investigated using scanning electron microscope. Smaller sized particles will have better movement between electrodes and thereby increasing the performance. Samples have suffered capacity loss over multiple cycles, which might be due to impedance growth over the cathode material. A detailed impedance spectroscopy can be conducted on the materials to observe the change of resistance buildup during cycling which results in capacity loss. Rietveld refinement can be performed on the powder diffraction data to get a better idea on structural data like structural stability of the material[25].

The repeat sample#1 showed better performance when cooked under argon during second heating. Further experimentation is needed to see if the contamination of the material during normal cooking resulted in poorer performance than cooking in argon.

As a future work on samples 1, 18 and 20 high resolution XPS scans can be performed to conduct a clear analysis. With better XRD scans performed on these samples, a Rietveld

refinement can be performed to see if there are any minute impurities which might have caused the inconsistency in the repeats. For further exploration of rogue phases in the materials, an argon beam line high resolution TEM can be performed.

## References

1. Masaki Yoshio, R.J.B., Akiya Kozawa, *lithium ion batteries: Science and technologies*. Springer2009.
2. darden, B. *Battery manufacturers and Brand Names*. 2002; Available from: [http://docs.zetataalk.com/Batteries/Types/Bat\\_Brand\\_2004.pdf](http://docs.zetataalk.com/Batteries/Types/Bat_Brand_2004.pdf).
3. Armand, J.-M.T.M., *Issues and Challenges facing rechargeable lithium batteries*. nature, November 2001. **414**: p. 359-367.
4. srinivasan, v., *Batteries for vehicular applications*, 2008, NREL: Berkley.
5. Linden, D. and T.B. Reddy, *Handbook of Batteries (3rd Edition)*, 2002, McGraw-Hill.
6. Scrosati, B., *Recent advances in lithium ion battery materials*. Electrochimica Acta, 2000. **45**(15-16): p. 2461-2466.
7. Kim, W.-S. and W.-Y. Yoon, *Observation of dendritic growth on Li powder anode using optical cell*. Electrochimica Acta, 2004. **50**(2-3): p. 541-545.
8. Wakihara, M., *Recent developments in lithium ion batteries*. Materials Science and Engineering: R: Reports, 2001. **33**(4): p. 109-134.
9. Cuenca, L.G.a.R., *Costs of Lithium-Ion Batteries for Vehicles*, 2002, Argonne National Laboratory: illinois.
10. Julien, C., et al., *Studies of LiNi<sub>0.6</sub>Co<sub>0.4</sub>O<sub>2</sub> Cathode Material Prepared by the Citric Acid-Assisted Sol-Gel Method for Lithium Batteries*. Journal of Sol-Gel Science and Technology, 1999. **15**(1): p. 63-72.
11. Betco, C., *The a-hydroxide precursor preperation and electrochemical properties of LiNi<sub>0.8</sub>Co<sub>0.15</sub>Al<sub>0.05</sub>O<sub>2</sub>*. New energy material chemistry.
12. Zhang, L., Takada, K, Ohta, N, Fukuda, K, Osada, M, Wang, LZ, Sasaki, T and Watanabe, M, *Layered (1-x-y)LiNi<sub>1/2</sub>Mn<sub>1/2</sub>O<sub>2</sub> center dot xLi[Li<sub>1/3</sub>Mn<sub>2/3</sub>] O-2 center dot yLiCoO(2) (0 <= x = y <= 0.3 and x=0.5) cathode materials*. Journal of The Electrochemical Society, 2005. **152**(1): p. A171-A178.
13. Lee, Y.-s., Y.-K. Sun, and K.-S. Nahm, *Synthesis of spinel LiMn<sub>2</sub>O<sub>4</sub> cathode material prepared by an adipic acid-assisted sol-gel method for lithium secondary batteries*. Solid State Ionics, 1998. **109**(3-4): p. 285-294.
14. Peng, Z.S., C.R. Wan, and C.Y. Jiang, *Synthesis by sol-gel process and characterization of LiCoO<sub>2</sub> cathode materials*. Journal of Power Sources, 1998. **72**(2): p. 215-220.

15. <http://gigaom.com/cleantech/how-ultracapacitors-work-and-why-they-fall-short/>
16. "Vehicle of Change," Lawrence Burns, Byron McCormick, and Christopher Borroni- , Scientific American, Vol. 287, Issue 4, 10/02
17. Inductively Coupled Plasma - Atomic Emission Spectrometry  
By **THOMAS J. MANNING\*** AND **WILLIAM R. GROW**
18. <http://www.greencarcongress.com/2009/03/doe-to-award-up-to-24b-for-advanced-batteries-electric-drive-components-and-electric-drive-vehicle-d.html>
19. Y. Wu and A. Manthiram, Electrochemical society. Solid-state letters, Volume 9, Issue 5, pages A221-A224 (2006)
20. Y.Sun, Y. Xia, Y.Shiosaki and H. Noguchu, Preparation and electrochemical properties of  $\text{LiCo}_2\text{-LiNi}_{0.5}\text{Mn}_{0.5}\text{O}_2\text{-Li}_2\text{MnO}_3$  solid solutions with high Mn contents
21. Robert A. Huggins, Advance Batteries Materials Science Aspects
22. M.Stanley Whittingham, Lithium Batteries and Cathode Materials, Chem. Rev 2004, 104.
23. A.K.Padhi, K.S. Nanjundaswamy and J.B.Goodenough, Phospho-olivines as Positive-Electrode Materials for Rechargeable Lithium Batteries.
24. Alcantara, R.; Lavela, P.; Tirado, J.L.; Zhecheva, E.; Stoyanova, R. Recent advances in the study of layered lithium transition metal oxides and their application as intercalation electrodes. *J. SolidState Electrochem.* **1999**, 3, 121–134
25. C.Madhu, Joshua Garrett, Venkatesan Manivannan, Synthesis and characterization of oxide cathode materials of the system  $(1-x-y)\text{LiNiO}_2.x\text{Li}_2\text{MnO}_3.y\text{LiCoO}_2$
26. Guorong Hu, Wanmin Liu, Zhongdong Peng, Ke Du, Yanbing Cao, Synthesis and electrochemical properties of  $\text{LiNi}_{0.8}\text{Co}_{0.15}\text{Al}_{0.05}\text{O}_2$  prepared from the precursor  $\text{Ni}_{0.8}\text{Co}_{0.15}\text{Al}_{0.05}\text{OOH}$
27. Yucheng Sun, Chuying Ouyang, Zhaoxiang Wang, Xuejie Huang and Liquan Chen, Effect of Co content on Rate performance of  $\text{LiMn}_{0.5-x}\text{Co}_{2x}\text{Ni}_{0.5-x}\text{O}_2$  Cathode Materials for Lithium-Ion Batteries
28. Randolph A.Leising, Marcus J. Palazzo, Esther Sans Takeuchi, Kenneth J. Takeuchi, A study of the overcharge reaction of lithium-ion batteries
29. Zhonghua Lu, D.D.MacNeil, J.R.Dahn, Solid state letters, Volume 4 Issue 12
30. Iikyung Hwang, Chul Wee Lee, Jae Chang Kim, Songhun Yoon, Particle size effect of Ni-rich cathode materials on lithium ion battery performance